Admittance survey of type 1 coronae on Venus

Trudi Hoogenboom,[1] Suzanne E. Smrekar,[2] F. Scott Anderson,[3] and Greg Houseman[1]

Received 19 August 2003; revised 3 December 2003; accepted 15 December 2003; published 2 March 2004.

[1] In this study, we analyze Magellan gravity and topography data for Type 1 coronae on Venus to estimate crustal thickness (Z_c), elastic thickness (T_e), and apparent depth of compensation (Z_L). We examine the free-air admittance for all 103 Type 1 coronae (defined as having greater than 50% complete fracture annuli) that are resolved in the gravity data. A spatio-spectral method is used to calculate a localized admittance signature of each corona from a global admittance map. This method extracts spectral information from a region in space whose area is varied as a function of degree to make it large enough to yield robust results at every individual wavelength. Elastic flexure models with either bottom- or top-loading compensation are used to fit the data. The estimated lithospheric flexural parameters span the range obtained for other topographic features on Venus, suggesting that the lithosphere on which coronae form is variable. We find no significant difference in lithospheric properties between Type 1 and 2 coronae. Fifty-four percent of all coronae are consistent with local isostasy, which may indicate that they are no longer active. Very few coronae with dome or plateau morphologies have a bottom-loading signature or the small T_e and large Z_L expected if a mantle plume were present. Approximately 71% have Z_L estimates less than 70 km, indicating that compensation probably occurs within the crustal layer. We find no systematic relationship between T_e or Z_c and corona diameter, as would be expected for the spreading-drop model of formation. *INDEX TERMS:* 5430 Planetology: Solid Surface Planets: Interiors (8147); 5475 Planetology: Solid Surface Planets: Tectonics (8149); 6295 Planetology: Solar System Objects: Venus; 8121 Tectonophysics: Dynamics, convection currents and mantle plumes; 8122 Tectonophysics: Dynamics, gravity and tectonics; *KEYWORDS:* Venus, corona, gravity, admittance

Citation: Hoogenboom, T., S. E. Smrekar, F. S. Anderson, and G. Houseman (2004), Admittance survey of type 1 coronae on Venus, *J. Geophys. Res.*, *109*, E03002, doi:10.1029/2003JE002171.

1. Introduction

[2] Coronae are roughly circular features unique to Venus that are defined primarily by their annular fractures. They may provide a potentially useful probe of lithospheric thickness since they deform the elastic lithosphere. The admittance between free-air gravity anomalies and topography can be used to estimate lithospheric parameters if we assume that the observed topographic and gravitational signals arise from the response of the elastic lithosphere to surface or sub-surface loading by flexure and regional isostatic compensation. Measurements of lithospheric properties derived from coronae may offer insights into differences in lithospheric structure or mantle convective pattern between Venus and Earth. A further goal of this study is to constrain coronae formation models.

[3] Of the 513 coronae on Venus [*Stofan et al.*, 2001; *Glaze et al.*, 2002], 406 are classified as Type 1 [*Glaze et al.*, 2002]. Type 1 are distinguished from Type 2 in that Type 1 coronae have greater than 180° of arc of fracturing (Figure 1). Type 1 coronae predominantly occur along chasmata and fracture belts settings. Type 2 coronae are more likely to be found isolated from other features [*Stofan et al.*, 2001].

[4] Our study follows recent investigations of gravity signatures associated with coronae [*Johnson and Richards*, 2003; *Smrekar et al.*, 2003; *Smrekar and Stofan*, 2003]. Previous studies have examined coronae morphology, size, fracture patterns, lithospheric properties, loading signature and geologic characteristics [e.g., *Smrekar et al.*, 2003]. However, these studies have either been limited to Type 2 coronae (coronae with <50% fracture annuli) [*Smrekar et al.*, 2003] or do not include bottom-loading compensation models [*Johnson and Richards*, 2003]. Coronae crustal thickness and elastic properties remain poorly constrained.

[5] In this study, we apply a similar methodology to that used by *Smrekar et al.* [2003] to determine whether systematic trends in elastic thickness and apparent depth of compensation are observed in Type 1 coronae. We further look for any correlation between lithospheric parameters or loading signature and corona morphology and compare these results to a study of Type 2 coronae [*Smrekar et al.*, 2003]. The lithospheric parameters are then compared with predictions made by different corona formation models including the spreading-drop [*Koch and Manga*, 1996] and plume-delam-

[1]School of Earth Sciences, University of Leeds, Leeds, UK.
[2]Jet Propulsion Laboratory, California Institute of Technology, Pasadena, California, USA.
[3]Hawaii Institute of Geophysics and Planetology, University of Hawaii at Manoa, Honolulu, Hawaii, USA.

0148-0227/04/2003JE002171$09.00

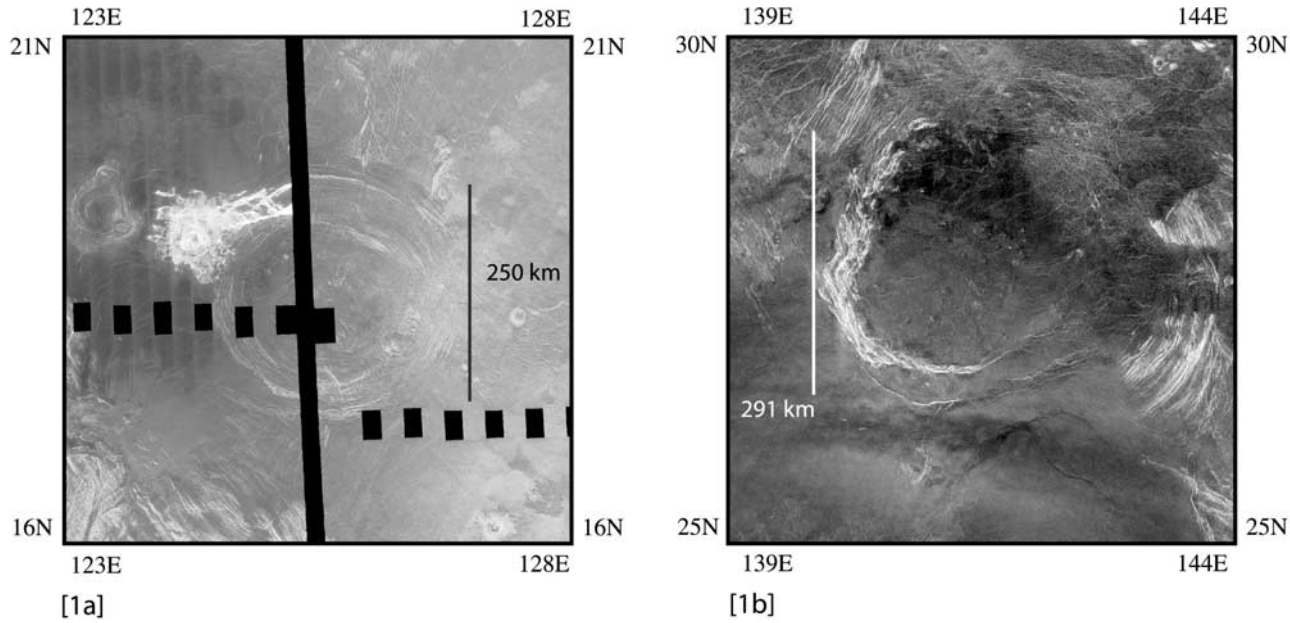

Figure 1. An example of a Type 1 dome shaped corona "Kapenopfu" (~250 km diameter) is provided in (a). Note the almost complete circular fracture rim. An example of a rim-only shaped Type 2 corona (approximately 290 km in diameter) is shown in (b). These synthetic aperture radar images were obtained by the Magellan mission (http://pdsmaps.wr.usgs.gov/maps.html).

ination [*Smrekar and Stofan*, 1997] models. These models are described in more detail in the discussion. A global admittance map [*Anderson and Smrekar*, 2001] was used to calculate the admittance signature for each corona. Both bottom and top-loading compensation models are used to derive lithospheric parameters [*McNutt*, 1983; *Forsyth*, 1985; *Anderson and Banerdt*, 2000].

2. Methods

2.1. Gravity and Topography Data

[6] Gravity data were acquired by Magellan (1990–1994) over 98% of Venus at an altitude of 155–220 km, providing a half wavelength resolution of ~100 km. We use the 180th degree and order spherical harmonic gravity field described by *Konopliv et al.* [1999]. Computation of admittance spectra also requires topography in a spherical harmonic representation. We use the spherical harmonic topography field described by *Rappaport et al.* [1990], complete to degree and order 360. Errors in the topography data are disregarded as the topography field is more accurate than the gravity field by more than two orders of magnitude.

[7] This study includes all 103 Type 1 coronae resolvable relative to the local error in the gravity field. The small average diameter of coronae (~210 km) results in many coronae gravity signatures below the nominal resolution of the data. We therefore only examine coronae with a diameter greater than the minimum resolvable wavelength (>200 km). Of the 207 coronae with diameters greater than 200 km, 49 were eliminated because their diameters were less than half the local degree strength. Degree strength provides an approximate gauge of data resolution and is defined as the spherical harmonic degree at which the power in the gravity field equals the power in the noise [*Konopliv et al.*, 1999]. For most coronae we can resolve the admittance spectra to degree 80. A further 29 coronae were removed because their local degree strength was less than 65. The remaining 129 coronae were examined using the spatio-spectral admittance method described by *Simons et al.* [1997]. Of these, 26 were eliminated due to large error estimates discussed further in the text.

2.2. Admittance

[8] The admittance $Q(k)$ is defined as the transfer function between the spectral representation of gravity $G(k)$ and topography $H(k)$:

$$\mathrm{G(k)} = \mathrm{Q(k)}*\mathrm{H(k)} + \mathrm{N(k)} \quad (1)$$

$N(k)$ is the uncorrelated noise in the data (assumed to be small) and k is the two-dimensional wave number ($2\pi/\lambda$) where λ is the wavelength. Following *Dorman and Lewis* [1970], we assume that the Venusian lithosphere is locally homogeneous and azimuthally isotropic. While various authors have studied the anisotropy of the terrestrial elastic lithosphere [e.g., *Simons et al.*, 2000], simple first order models (such as the ones used here) work well in modeling terrestrial elastic flexure and also enable the use of spectral methods.

[9] The admittance spectrum is sensitive to bending of the elastic lithosphere in response to a load from above, below or both. Admittance is therefore sensitive to elastic thickness (T_e) because elastic thickness controls the surface response of the load [*Watts et al.*, 1980]. The admittance varies depending on whether the topography is supported by the strength of the elastic lithosphere or by sub-surface density variations [*Banks and Swain*, 1978; *Forsyth*, 1985].

2.3. Spatio-Spectral Admittance

[10] We use the spatio-spectral localization approach of *Simons et al.* [1997] to calculate admittance estimates at

coronae locations. The spatio-spectral localization method is similar to a wavelet transform in that it extracts spectral information from a region localized in space and finds a compromise between spectral resolution and spatial localization. The spherical harmonic fields of gravity and topography are localized about a given location using a tapered spherical cap (or window), whose co-latitudinal size is proportional to wavelength. The product of the co-latitudinal size of the spherical cap and the width of the spectral component to be analyzed influences the spectral resolution of the estimate, just as the time-bandwidth product varies in the multitaper method discussed by *Simons et al.* [2000].

[11] Coefficients of the windowed field are used to calculate the admittance at that location. This method extracts spectral information from a region centered on the corona whose area varies as a function of degree to make it large enough to yield robust results at every individual wavelength [*Simons et al.*, 1994, 1997]. As such, the method is appropriate for calculating the admittance of relatively small (corona-size) features which are often found in association with other short-wavelength features.

[12] The window specification determines the trade-off between spectral and spatial localization. *Simons et al.* [1997] derive the relationship between spectral and spatial information for a window made up of the first lobe of a spherical harmonic cap of degree l. The spatial and spectral window widths are inversely related [*Simons et al.*, 1997]. The parameter f_s is used to control the spatial or spectral dominance for all spherical degrees. Low spatial resolution can be achieved using low f_s values, which reduces the local spectral bias and enhances the maximum degree to which the localization can be performed.

[13] Using spatio-spectral methods, the spectral resolution in harmonic degree degrades with increasing degree number but the spatial resolution improves. This approach contrasts with space-frequency methods like the multitaper methods used by *Simons et al.* [2000], in which the spatial size of the window is constant, but its shape is chosen to optimize retrieval of spectral information with the same local leakage or bias.

[14] Following *Simons et al.* [1997], the shortest wavelength that can be resolved within the chosen spherical harmonic window is

$$\lambda_{spectral} = \frac{2\pi R}{\sqrt{L_{nyq}(L_{nyq}+1)}} \tag{2}$$

where R is the radius of Venus (6051.9 km) and the Nyquist degree is

$$L_{nyq} \cong L_{obs} \cdot \frac{f_s}{(f_s+1)} \tag{3}$$

L_{obs} defines the degree strength of the field and f_s is the number of wavelengths that fit in the window. For Venus, the gravity field is resolved to degree $L_{obs} \cong 120$ [*Konopliv et al.*, 1999]. To maximize the resolution of local features we use a scaling parameter of $f_s = 2$ as such the co-latitudinal extent of the spherical cap increases linearly. Using equation (3), a value of $L_{nyq} = 80$ is obtained. For most coronae we can therefore resolve the admittance spectra to degree 80 or wavelength ~470 km. Thus a corona as small as 235 km, may be resolved as it has a spectral signature at twice its diameter.

[15] After convolving gravity and topography harmonics with the window coefficients, the localized admittance function is calculated by dividing the covariance of topography and gravity by the covariance of topography with itself (similar to the Cartesian approach). Each covariance is computed for all harmonics ($l \leq L_{nyq}$) with the window centered on a spherical domain Ω (in our case each corona) and summed over all tesseral harmonic fields (m) [*Simons et al.*, 1997].

[16] *Anderson and Smrekar* [2001] and *Smrekar et al.* [2003] used the spatio-spectral method to calculate a global admittance map. The admittance spectrum is calculated with its centre at the midpoint of a 1×1 degree spatial grid which incorporates all spectra within the co-latitudinal extent of the spherical cap. While there is considerable overlap in the spectral content for two adjacent regions, the short wavelength information changes smoothly due to the spectral nature of the data.

[17] From the global admittance map, we calculate the average admittance spectra of those points inside a square region encompassing the corona. The mean spectrum is then compared with compensation models assuming an elastic lithospheric layer. An automated routine calculates the best fit between the observed average admittance and the compensation model, over a specified wavelength range (generally $40 \leq l \leq 80$). The upper bound of the range depends on the local degree strength. The lower bound (degree 40) is chosen following *Nimmo and McKenzie* [1996], who suggest that any gravity signal at wavelengths longer than 1000 km cannot be due to elastic effects. Model fits are iteratively compared to the observed spectra, and the minimum misfit found by varying T_e and Z_c by increments of 5 km and Z_L by increments of 10 km. The range of T_e values considered for top-loading ($0 < T_e < 125$ km) and bottom-loading ($0 < T_e < 100$ km) was chosen to incorporate the range of T_e estimates (6 to 80 km) obtained from a variety of previous studies [e.g., *Sandwell and Schubert*, 1992; *Johnson and Sandwell*, 1994]. The range of crustal thickness values considered ($0 < Z_c < 100$ km) was chosen to incorporate the range of Z_c values obtained from previous theoretical, geodynamic and gravity studies reviewed by *Grimm and Hess* [1997]. The range of Z_L values considered for bottom-loading is between $30 < Z_L < 200$ km.

[18] Our method differs from that of *Smrekar et al.* [2003] in that we fit a mean spectrum for each corona as opposed to determining admittance classes. The class method used by *Anderson and Smrekar* [2001] and *Smrekar et al.* [2003] identifies, groups and averages spectra that are associated with the corona. The total spectra are thereby reduced to a limited set of representative classes. Using the class method, multiple average spectral classes were sometimes associated with a single corona. The mean spectrum method used here allows lithospheric parameters to be more precisely defined for individual coronae as the class method averages in spectra outside the coronae that are similar but not identical.

[19] *Smrekar et al.* [2003] compare the results obtained with the spatio-spectral admittance method to those calculated with a Cartesian method. In most cases, the two methods show reasonable agreement between the allowable

parameter ranges, although there are several discrepancies for the coronae examined. The main difference between the Cartesian and the spatio-spectral method used here is the fact that in the Cartesian case the same box size is used for all harmonics, whereas with the spatio-spectral method, the spherical cap changes size with the degree under investigation. Thus the agreement of the admittance spectra depends on the spatial homogeneity of the regions sampled. Exact agreement cannot be expected in most regions [*Smrekar et al.*, 2003]. Given that coronae are often found in close association with small volcanoes and other coronae, the Cartesian admittance signature may reflect the signatures of features other than the corona.

2.4. Compensation Models

[20] The interpretation of gravity data is fundamentally non-unique in the absence of significant additional constraints. However, on Earth, simple two-layer mechanical models of the lithosphere provide acceptable first-order interpretations of the lithosphere [*McNutt*, 1983; *Forsyth*, 1985]. Following this work, we use two simple top and bottom loading mechanical models to interpret the observed admittance functions of the Venusian lithosphere.

[21] We assume that the lithosphere comprises two laterally homogenous layers: Crust of thickness Z_c and mantle lithosphere of thickness Z_L, which are loaded by a harmonically varying topography, either at the surface (top-loading) or at a compensation depth below the crust-mantle interface (bottom-loading). The lithosphere is assumed to be in static equilibrium with stresses supported by elastic flexure of the uppermost elastic layer, thickness T_e. As T_e approaches 0, we obtain the limit of local isostatic compensation. At short wavelengths, a corona may have a predominantly bottom-loading, top-loading or isostatic signature. In some cases it is possible to distinguish top from bottom loading. We compare the predicted admittance from both top and bottom loading models to the observed admittance.

[22] The standard transfer function between free-air gravity anomalies and topography for loading of the elastic lithosphere from above (top-loading) is given by *Banks and Swain* [1978]:

$$Q_T(k) = 2\pi\rho_c G\left[1 - e^{-kZc}/\left(1 + Dk^4/\Delta\rho g\right)\right] \quad (4)$$

where $k = \sqrt{l(l+1)}/R$ is the horizontal wave number, G is the gravitational constant, Z_c is the thickness of the crust, g is surface gravity (8.87 ms^{-2}) and $\Delta\rho = \rho_m - \rho_c$ is the density contrast at the crust-mantle boundary. In all models, crustal and mantle densities of 2800 kg/m^3 and 3300 kg/m^3 are assumed respectively. The flexural rigidity (D) is defined by

$$D = \frac{ET_e^3}{12(1-\nu^2)} \quad (5)$$

with nominal parameter values of E, Young's modulus (10^{11} Pa) and ν, Poisson's ratio (0.25). Effective elastic thickness depends primarily on temperature, composition and state of stress of the lithosphere [*Lowry and Smith*, 1995] but could also depend on the orientation of the load. The inferred value of T_e may therefore represent an average of potentially inhomogeneous and anisotropic variation of these properties [*Lowry and Smith*, 1994].

[23] A top or bottom-loading signature implies that the topography is at least partially compensated by flexure of the elastic lithosphere. Local isostasy ($D \rightarrow 0$) indicates that the region is compensated by variations in the layer thickness that balances the surface topography. Under isostatic conditions, the admittance is

$$Q_T(k) = 2\pi\rho_c G\left(1 - e^{-kZ_c}\right) \quad (6)$$

[24] From *McNutt* [1983], *Anderson and Banerdt* [2000] derive the spherical harmonic representation of the admittance resulting from a load at depth (bottom-loading):

$$Q_N = 2\pi G\left[\rho_c + (\rho_m - \rho_c)e^{-kZc} - \left(\left(Dk^4 + \rho_m g\right)/g\right)e^{-kZL}\right] \quad (7)$$

This bottom-loading equation includes a crustal interface and a second density interface at depth, Z_L, below the crust mantle boundary. Apparent depth of compensation (Z_L) defines the depth above which the mass of the topography is balanced by a compensating mass at depth. As crustal thickness cannot be constrained independently of the apparent depth of compensation using only gravity and topography data, we assume a crustal thickness of 30 km for the bottom-loading model and use the model to constrain elastic thickness and apparent depth of compensation (Z_L). A value of 30 km is chosen, given that previous studies using gravity data indicate that the mean thickness of the crust is 20 to 50 km [*Grimm and Hess*, 1997, and references therein]. A number of previous workers have estimated that the crustal thickness in the northern plain of Venus is at most 30 km [e.g., *Zuber and Parmentier*, 1990, and references therein]. In addition, the average crustal thickness for all coronae best fit with a top-loading model is ~38 km. Using a larger crustal thickness value, results in a larger value of apparent depth of compensation.

[25] The shape of the admittance as a function of wavelength is sensitive to whether the elastic lithosphere is flexing in response to a load applied at the surface (top-load) or at depth (bottom-load). For short-wavelength loads at depth, the free-air admittance slope is negative because the amplitude of the gravity anomaly decreases faster than that of the topography anomaly (Figure 2a). For a surface load, the free-air admittance has a positive slope at short wavelengths because the gravity anomaly due to the surface load remains significant while the topography signal decreases with wave number (Figure 2b). For a comparison of the differences between free-air and Bouguer gravity calculations, the reader is referred to *McKenzie* [2003].

[26] While the slope of the admittance versus degree graphs can indicate whether top or bottom-loading or isostasy is the preferred interpretation, explanation of these loading signatures is not straightforward. A variety of processes can cause the elastic lithosphere to be loaded from above or below. A bottom-loading signature implies that a low density mass, (e.g., plume) is pushing up on the base of the lithosphere creating a topographic high. Alternatively a high density mass (or downward flow in the mantle) pulls the lithosphere down creating a topographic low. A region exhibiting a top-loading signature may be explained by a surface mass (e.g., volcano) depressing the

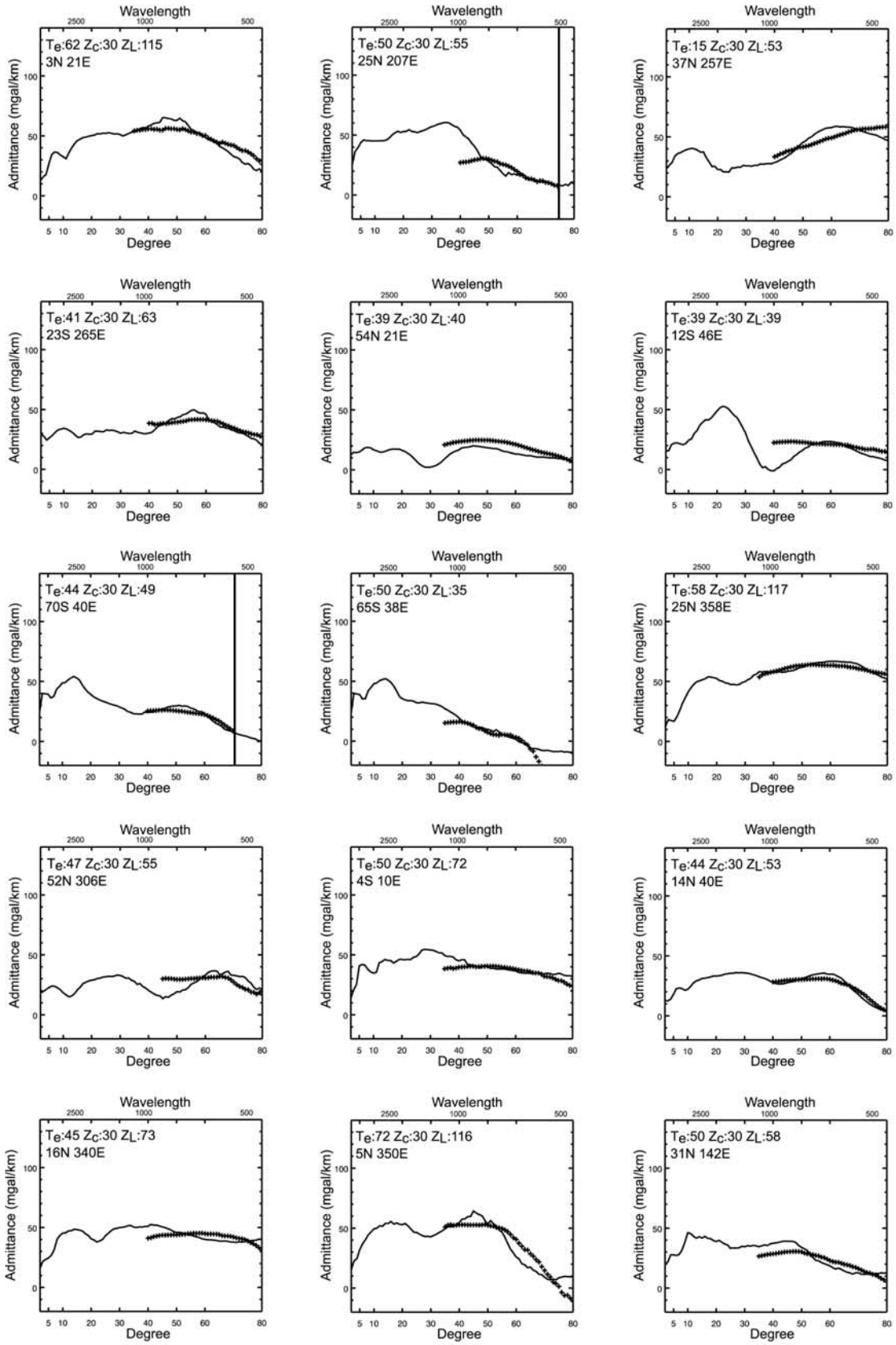

Figure 2a. Spatio-spectral admittance spectra (solid lines) for 15 coronae fit with a bottom-loading model. The best fit values of T_e and Z_L are given in the upper left. Best fit theoretical admittance functions are shown as crosses. The vertical line represents the degree strength in the region of each corona.

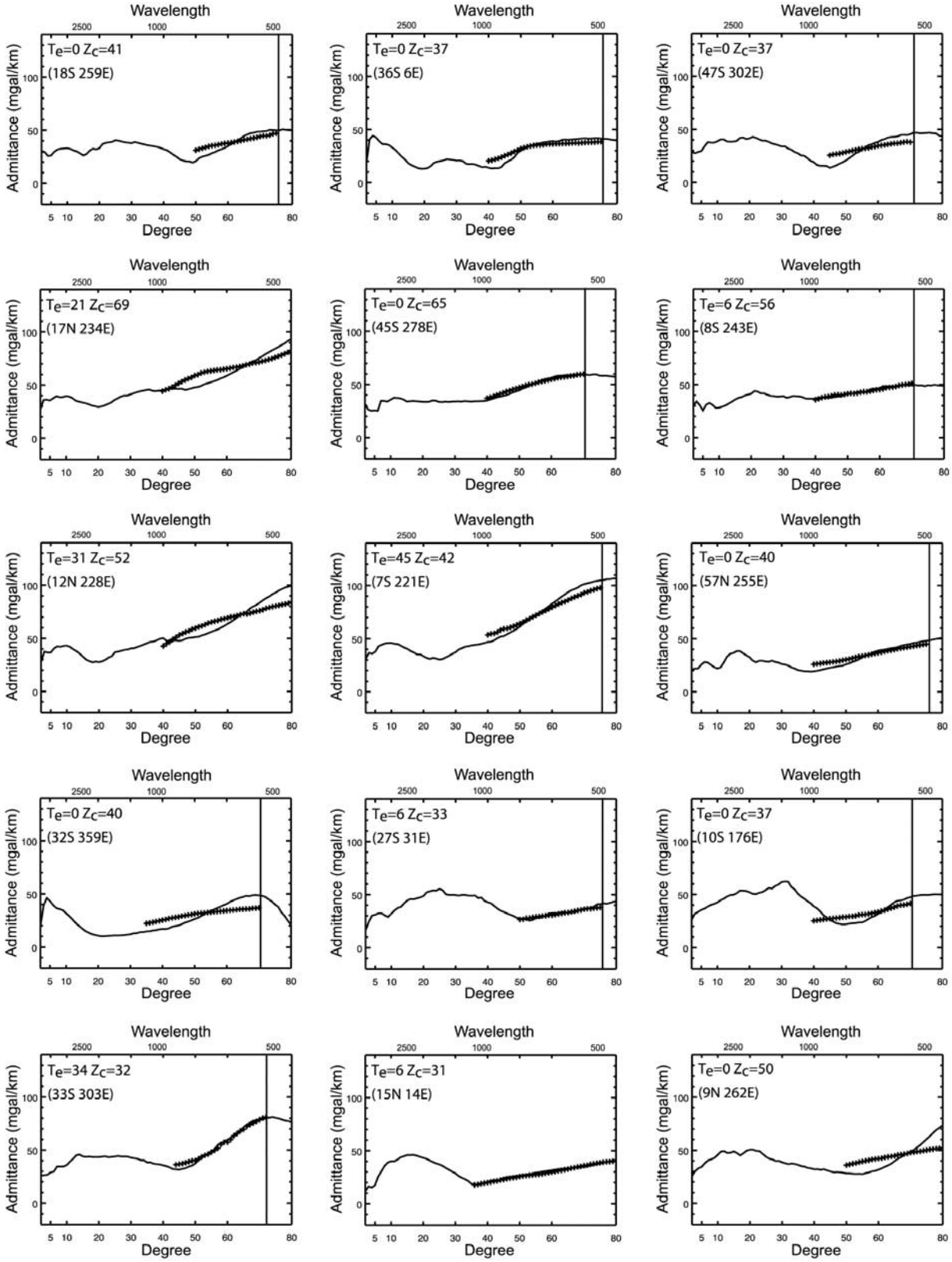

Figure 2b. Spatio-spectral admittance spectra for 15 coronae fit with a top-loading model. The best fit values of T_e and Z_c are given in the upper left. Best fit theoretical admittance functions are shown as crosses. The vertical line represents the degree strength in the region of each corona.

original topography as the elastic plate flexes. In many cases, however, there is no obvious surface load. While some coronae contain large domes (~100 km in diameter) capable of causing significant lithospheric deflection, most coronae have distributed volcanic flows that are not expected to produce the same type of focused load as a shield volcano [*McGovern and Solomon*, 1998].

[27] Top and bottom-loading elastic flexure signatures can also be mimicked by dynamic processes in a viscous mantle. *Smrekar and Stofan* [1999] showed that the gravity signature of a corona with a delaminating lower lithosphere is similar to a top-loading signature because the topography is pulled downward as the load depresses the surface. A mantle plume can also produce a top-loading signature, as shown by *Smrekar et al.* [1997] for a larger scale plume. In reality, dynamic stress associated with flow in the mantle, and static stress associated with variations in crustal layer thickness, may only be partially supported by elastic strain in the lithosphere, and therefore terms such as "bottom-loading" or "top-loading" may signify no more than convenient descriptive labels for the classification of observed admittance spectra. Despite these complications, these first-order models are effective in describing elastic flexure on Earth [e.g., *McNutt*, 1983]. In the absence of other constraints, we apply these models to interpret the observed admittance functions of coronae on Venus.

[28] Numerous studies have addressed the question of the importance of sub-surface loading on estimates of T_e. *Forsyth* [1985] found that internal loading has an important effect on values of the admittance, and argued that the effect of variation of f (the ratio of the internal to the surface load) on estimated values of T_e could be reduced using the coherence between Bouguer gravity and topography. Coherence provides a measure of the statistical relationship between gravity and topography and is relatively insensitive to the effects of top and bottom-loading and to errors in the depth of sub-surface loading [*Forsyth*, 1985]. The method generally assumes that top- and bottom-loading processes are uncorrelated. Estimates of T_e obtained using Forsyth's method have provided values as large as 130 km for continental lithosphere [*Zuber et al.*, 1989]. Note that except for a few isolated regions, gravity data for Venus does not have adequate resolution to permit coherence studies.

[29] *McKenzie and Fairhead* [1997] argue that such large values of T_e are incompatible with pressure and temperature estimates from the mineralogy of mantle nodules. They estimated T_e from free-air (rather than Bouguer) admittance and found much smaller values which they attributed to the existence of large sub-surface density anomalies that are not expressed in the surface topography [*McKenzie*, 2003]. Other studies [e.g., *Simons et al.*, 2000; *Banks et al.*, 2001] suggest that more reliable (larger) T_e estimates are obtained when sub-surface loading is explicitly represented. *McKenzie and Fairhead* [1997] discuss the importance of comparing the spectral power of the free-air gravity anomaly with the power in that part of the gravity anomaly due to surface topography. *McKenzie and Fairhead* [1997] and *Wang and Mareschal* [1999] show figures of the relative power in the topography-derived Bouguer correction versus the power in the total gravity anomaly, and use this as an indicator for the presence of sub-surface loading.

2.5. Error Analysis

[30] Several factors contribute to the uncertainty in the inferred flexural parameters. These include data noise, method biases and the occurrence of processes other than flexural and isostatic adjustment of homogenous layers [*Smrekar et al.*, 2003]. In this analysis, noise is represented as scatter in the admittance and is not considered explicitly, however several studies address the importance of noise on the estimation of elastic thickness. For example, *Banks et al.* [2001] investigate the effect of sub-surface lateral density contrasts on the estimation of continental elastic lithospheric thickness.

[31] Recent studies have also addressed the importance of method biases on estimation of T_e. *Lowry and Smith* [1994] compare the periodogram method (a classical Fourier transform technique), with the maximum-entropy method, which attempts to reduce the effects of windowing on data. *Simons et al.* [2000] compare the periodogram method with the multitaper method and suggest that the multitaper method is more robust at low wave numbers because it allows for many independent estimates of this isostatic response that are minimally affected by spectral leakage.

[32] A significant source of uncertainty arises from the lack of independent constraint on crustal thickness and density. *Lowry and Smith* [1995] discuss model parameter uncertainties calculated from terrestrial admittance studies. We account for these uncertainties following the approach adopted by *McKenzie and Fairhead* [1997], and quote parameter ranges corresponding to 2 times the observed RMS error in the average admittance. In this study we found that we could constrain the lithospheric parameters to 1.5 times the observed RMS. For each corona, we assume that the variation in admittance values in the target region is representative of the uncertainty in admittance and is equal to 1.5 or 2 times the standard deviation about the mean:

$$RMS_l = \frac{1}{N_{ADM}} \left[\sum (x_l - \mu)^2 \right]^{\frac{1}{2}} \tag{8}$$

where μ is the mean corona admittance, x_i is the admittance at degree l and N_{ADM} is the number of admittance signatures averaged over.

[33] An average admittance error for each corona is then defined by

$$RMS = \frac{1}{N_l} \sum_l RMS_l \tag{9}$$

where N_L is the number of degrees for which a compensation model is fit.

[34] Eight coronae were found to have average error values greater than 20 mgal/km and were eliminated. Another seven coronae had model fit errors that were too large (>13 mgal/km) to adequately represent the observed admittance. A further 8 coronae were removed because the range of allowable lithospheric parameters were unconstrained (T_e and Z_c ranges greater than 70 km). Four of the coronae showed admittance spectra that are too flat to determine if the best fitting model is isostatic, bottom-loading or top-loading. These spectra had up to a factor of

two less power, in gravity and topography, compared to those of the majority of coronae.

3. Results

[35] The majority of coronae (approximately 63%) can be interpreted in terms of a top-loading model. The remaining 37% were interpreted as bottom-loaded. The derived lithospheric parameters for coronae fit using a bottom-loading model are provided in Table 1 and those fit by a top-loading model in Table 2. At smaller values of T_e (<15 km) top and bottom-loading models are indistinguishable across the degree range we examine, and both are closely approximated by an isostatic admittance signature. In total, 54% displayed admittance signatures indistinguishable from an isostatic signature. 28% were only fit with a bottom-loading model and 18% were only fit with a top-loading model. The spatio-spectral admittance spectra and best fit model spectra for a selection of 30 coronae are shown in Figures 2a and 2b. For the 38 coronae fit using a bottom-loading model, the range of best fit elastic thickness values is 0–73 km, with a mean and standard deviation of 39 ± 19 km. The apparent depth of compensation ranges from 30 to 117 km, with a mean and standard deviation of 63 ± 28 km. A top-loading model was used to fit spectra for 65 coronae. The resulting T_e estimates range from 0 to 48 km, with a mean and standard deviation of 12 ± 15 km. Crustal thicknesses between 2 and 69 km were inferred, with a mean and standard deviation of 38 ± 19 km. Removing the coronae interpreted to be isostatic from this group has little effect on the mean, standard deviation and range of Z_c and Z_L.

3.1. Estimates of Error

[36] The error plots shown in Figures 3a and 3b illustrate the range of acceptable lithospheric parameters for the same 30 coronae with the best fit values of T_e, Z_c, and Z_L reported in Tables 1 and 2. The acceptable ranges for T_e, Z_c and Z_L are those for which the RMS misfit is within 1.5 times the estimated RMS variation of the observed admittance. Tables 1 and 2 show the parameter ranges for data fit within both 1.5 and 2 times the observed RMS following *McKenzie and Fairhead* [1997]. For top-loading models, the mean uncertainty for T_e is 11 km and that for Z_c is 16 km. Bottom-loading models display a mean uncertainty of 21 km for T_e and 23 km for Z_L. The range for bottom-loading models may be larger because any error in the assumed value of Z_c will influence the inferred value of Z_L. The parameter ranges derived using this estimate of uncertainty are larger than those discussed by *Barnett et al.* [2000] due to differences in the methods used to calculate admittance [*Smrekar et al.*, 2003]. A more detailed description of the differences between our method and that used by *Barnett et al.* [2000] is provided by *Smrekar et al.* [2003]. The parameter ranges for which the misfit is twice the observed RMS variation are as much as a factor of two larger than those for which the misfit is 1.5 times the observed RMS.

4. Discussion

4.1. Elastic Thickness and Isostasy

[37] Elastic thickness estimates of planetary lithospheres have been obtained from modeling topographic profiles across coronae trenches assumed to be flexural [*Sandwell and Schubert*, 1992; *Johnson and Sandwell*, 1994], from topography profiles across large coronae [*Brown and Grimm*, 1996] and from previous models of coronae admittance spectra [*Barnett et al.*, 2000; *Smrekar et al.*, 2003]. These studies provide estimates of T_e between 6 and 80 km. Estimates of elastic thickness obtained from admittance studies for a variety of Venusian features [*McKenzie and Nimmo*, 1997; *Simons et al.*, 1997; *Barnett et al.*, 2000] range from 10 to 65 km. Consistent with those earlier studies, T_e estimates found here range between 0 and 73 km.

[38] For the majority of coronae with a top-loading signature, and for 18% of coronae best fit with a bottom-loading signature, an isostatic model provides an equally good fit. 30% of the coronae examined are best fit with an elastic thickness of 0 km. A further 24% have a best fit elastic thickness less than 20 km and include 0 km in their range of uncertainty. We interpret these low T_e values to indicate isostatic compensation. Isostatic compensation implies that the topography is supported by sub-surface density variations, typically interpreted as crustal thickness variations. In these regions, loading stresses in the elastic lithosphere have relaxed and little if any of the load is compensated by elastic flexure or by dynamic processes. In addition to density interface displacements, isostatic compensation may also result from temperature differences or compositional variation.

[39] If we eliminate the 53 coronae with isostatic or near-isostatic signatures, the range of T_e for top-loading models is 21–48 km. A top-loading fit is more influenced by power in the short wavelengths of the admittance functions and assumes no contribution from strength in the mantle [*Forsyth*, 1985; *Petit and Ebinger*, 2000]. Such models may therefore be biased toward smaller values of T_e. Bottom-loading models show a larger range of T_e values of 32–73 km. Terrestrial investigations that have examined both compensation models also indicate larger values for bottom-loading [e.g., *Petit and Ebinger*, 2000]. Differences in analysis methods may also influence estimates of elastic thickness [see *Petit and Ebinger*, 2000].

[40] Elastic thickness calculations for 10 volcanoes on Venus by *McGovern and Solomon* [1998], and by *Kiefer* [2000], find values of T_e between 8 and 22 km. In agreement with a study of Type 2 coronae [*Smrekar et al.*, 2003], we find that this set of Type 1 coronae shows the full range of elastic thickness values observed elsewhere on Venus. The elastic thickness therefore does not appear to constrain the occurrence of Type 1 coronae.

4.2. Crustal Thickness (Z_c)

[41] Both the range of crustal thickness values obtained from top-loading models (6–69 km) and that for coronae interpreted to be isostatic (2–68 km) overlap with the range of 20–50 km determined in a variety of Venusian gravity studies for different geologic features, as summarized by *Grimm and Hess* [1997]. Coronae appear to form regardless of crustal thickness.

[42] Twelve coronae exhibit crustal thickness values less than 15 km. These coronae display elastic thickness estimates between 9 and 24 km, are located in different geologic settings and display a wide variety of topographic forms. Furthermore, eleven coronae display crustal thickness values greater than 60 km. Elastic thickness estimates

Table 1. Lithospheric Parameters Derived for 38 Coronae Interpreted Using a Bottom-Loading Model[a]

Lat., deg	Lon., deg	Diam., km	Geol. Setting	Topo. Gp	Best Fit T_e, km	T_e Range, km (1.5)	T_e Range, km (2.0)	Best Z_L, km (1.5)	Z_L Range, km (1.5)	Z_L Range, km (2.0)	RMS Fit, mgal/km	RMS Obs., mgal/km
3.5	21.5	400	FB	1	62	59–67	57–70	115	108–120	100–125	3.0	6.3
25.8	207.0	250 × 160	FB	1	50	29–55	16–57	55	34–65	28–72	1.4	8.8
37.0	257.0	280	FB	1	15	1–48	0–55	53	42–92	39–100	1.7	6.2
−23.5	265.5	380	FB	2	41	33–45	28–47	63	53–70	50–74	3.7	4.2
54.0	21.8	375	FB	2	39	27–45	19–53	40	31–48	28–58	7.2	6.1
−12.5	46.0	525	PL	2	39	17–53	0–56	39	25–58	13–64	3.5	9.2
−70.5	40.0	400	FB	2	44	39–50	36–52	49	44–56	42–58	1.6	2.9
−65.5	38.0	370	FB	2	50	43–54	41–57	35	28–42	27–45	1.2	4.0
25.0	358.0	230	RS	2	58	48–61	45–63	117	103–123	98–126	2.0	2.7
0.0	124.5	300	FB	3a	37	31–34	28–45	43	35–48	32–52	2.7	2.1
52.6	306.5	600	PL	3a	47	9–52	0–56	55	19–66	14–74	2.1	8.2
−4.3	10.0	250	FB	3a	50	42–54	33–57	72	64–83	50–89	3.1	4.3
14.3	40.2	500	RS	3a	44	41–47	39–57	53	49–56	46–58	1.5	3.0
16.0	340.0	310	PL	3a	45	37–50	21–54	73	63–81	45–87	3.4	5.2
5.0	350.0	375	PL	3b	72	67–76	64–79	116	110–124	106–130	1.7	8.6
31.5	142.9	553	PL	3b	50	44–54	30–57	58	48–64	35–70	3.5	6.1
6.0	20.0	300	RS	3b	45	36–49	33–52	79	67–87	64–91	1.3	3.8
19.0	98.0	380	FB	3b	44	37–48	34–50	55	49–61	47–65	1.1	5.7
−27.5	50.5	370	FB	3b	32	18–48	0–54	53	39–80	32–88	1.9	6.1
−25.5	269.0	250	FB	3b	41	31–47	25–47	53	44–59	40–62	1.8	5.2
−3.0	153.0	225	FB	3b	45	37–51	28–56	37	30–48	25–60	5.0	9.5
25.5	355.5	300 × 200	RS	3b	53	22–58	7–60	115	82–124	73–129	5.2	4.2
26.0	97.7	225	FB	3b	73	67–78	62–82	115	107–124	98–132	2.2	10.8
62.6	263.5	503 × 435	FB	3b	0	0–22	0–32	52	43–67	37–74	1.1	5.3
−8.5	47.0	525	FB	3b	39	25–51	14–55	41	31–59	28–65	3.4	8.6
6.5	43.5	575	RS	3b	50	48–52	46–53	94	91–97	88–100	1.3	0.1
−24.5	72.0	275	FB	3b	21	1–26	25–39	33	24–39	22–42	2.2	3.3
29.0	318.0	250	FB	4	62	58–66	34–68	115	109–119	67–124	1.7	6.2
12.5	24.0	350	FB	4	45	31–49	19–52	84	70–90	64–94	0.6	2.6
−22.5	57.0	450	FB	4	44	36–51	26–56	34	27–45	24–59	5.4	8.6
−22.8	259.6	380	FB	4	32	0–40	1–44	52	34–60	23–67	1.7	4.1
61.5	283.0	225	RS	4	0	1–41	0–50	49	38–77	35–89	0.7	7.1
9.0	315.5	220	PS	4	0	1–37	0–42	30	21–53	18–60	1.6	7.1
−63.5	322.5	300	FB	5	40	35–42	33–44	30	27–34	25–36	1.0	2.5
−46.0	56.0	250 × 175	FB	6	0	0–50	0–55	33	22–73	18–80	1.9	7.2
2.0	355.0	1060	PL	7	0	0–41	0–56	68	48–99	40–123	1.1	10.8
21.0	136.5	400	PL	7	38	21–50	0–53	42	28–58	20–65	1.2	7.9
−36.0	298.5	375 × 330	RS	7	44	42–45	37–47	60	57–61	50–65	0.3	1.0

[a]Latitude, longitude, and corona diameter are also shown. The geologic setting for each corona is also provided (TEssera, Fracture Belt, PLains, RiSe). Descriptions of topographic groups are provided in Table 3 and Figure 6. Ranges for T_e and Z_L are based on an RMS misfit of 1.5 times the estimated RMS admittance error. The parameters that lie within a range of 1.5 times the RMS for each spectrum are shown in the error plots in Figure 3a. For comparison with *Barnett et al.* [2000], ranges are also shown for 2.0 times the observed RMS error.

for these coronae range between 0 and 25 km. All of these coronae are located in fracture belt settings and display a wide range of annuli and topographic shapes. Large variations in inferred crustal thickness may result from density variations within the crust [*Smrekar et al.*, 2003] or from actual crustal thickness variations.

[43] Figure 4a shows the effect of varying crust-mantle density contrast on admittance spectra for top-loading models with a 25 km elastic thickness and a range of crustal thicknesses between 0 and 40 km. Solid lines represent a density contrast of 500 kg/m^3 as used in Figures 2a, 2b, 3a, and 3b, and bold dashed lines represent a smaller density contrast of 200 kg/m^3. For the two density contrasts shown in Figure 4a, the difference in admittance is up to ~20 mgal/km at the shortest wavelengths. Larger values of crustal thickness are less dependent on density contrast. At larger values of elastic thickness (40 km) (Figure 4b), the difference in crustal thickness is smaller and we observe that the admittance curves approach the asymptote as more of the load is flexurally compensated.

[44] Figure 4c shows the free-air admittance spectra for Pomona corona (79.3N 299.4E) along with the best fit admittance (T_e:18 km, Z_c:4 km) using a top-loading model with crust-mantle density contrast of 500 kg/m^3 (solid line). For comparison we include an alternative model fit using a density contrast of 200 kg/m^3 (dashed lines). Using the smaller density contrast, an elastic thickness of 10 km and a crustal thickness of 11 km provides a better fit at the smaller wavelengths associated with coronae-size features. Thus it is possible that those coronae for which we have determined very small crustal thickness values could be better fit by a smaller density contrast than the 500 kg/m^3 used here and a consequently greater crustal thickness.

4.3. Apparent Depth of Compensation (Z_L)

[45] In a dynamic mantle, the apparent depth of compensation is strongly dependent on lithospheric viscosity and mantle structure [*Moresi and Parsons*, 1995; *Smrekar et al.*, 1997] and is not simply interpreted as the depth to a thermal anomaly at the base of the lithosphere. Estimates of Z_L can however, be used to compare relative depths of compensation between coronae.

[46] The average Z_L value we obtain for coronae interpreted using a bottom-loading model is 65 km, and ranges

Table 2. Best Fit Lithospheric Parameters Derived for 65 Coronae Interpreted Using the Top-Loading Model[a]

Lat., deg	Lon., deg	Diam., km	Geol. Setting	Topo. Group	Best Fit T_e, km	T_e Range, km (1.5)	T_e Range, km (2.0)	Best Fit Z_c, km	Z_c Range, km (1.5)	Z_c Range, km (2.0)	RMS Fit, mgal/km	RMS Obs., mgal/km
−21.7	271.0	250 × 200	FB	1	24	22–27	17–32	6	3–9	0–25	6.3	4.3
73.3	261.4	653 × 391	RS	1	15	11–17	0–19	31	29–36	28–44	1.5	1.0
9.0	219.5	260	FB	1	0	0–5	0–8	60	54–66	52–68	3.9	1.1
8.5	214.0	275	FB	2	41	25–54	18–58	34	26–53	23–60	5.2	1.5
2.5	223.0	518	FB	2	35	29–39	28–40	37	34–43	33–54	2.9	1.2
17.8	240.0	350 × 300	FB	2	25	21–29	19–32	64	59–67	56–75	5.1	2.8
24.0	243.5	500 × 225	FB	2	22	14–27	0–36	62	57–73	50–90	4.8	3.2
−50.0	40.0	600	FB	2	0	0–6	0–12	55	58–68	43–68	9.8	7.4
22.0	224.0	350	FB	2	12	8–13	0–16	48	47–53	44–56	1.1	0.8
−37.0	288.0	500	RS	2	6	0–9	0–12	44	40–45	37–47	6.4	3.6
13.0	226.5	300	FB	2	1	0–11	0–16	68	59–77	54–83	4.1	3.8
−42.0	279.8	675	RS	2	0	0–5	0–7	63	62–68	60–69	2.9	0.9
12.0	221.0	850	FB	2	0	0–5	0–7	61	59–65	57–67	2.3	1.0
−5.5	251.2	450	FB	2	21	16–23	14–24	38	35–42	35–53	3.4	1.8
19.5	227.5	350	FB	2	0	0–5	0–13	49	46–54	36–63	7.0	1.5
−18.5	259.0	225	FB	2	0	0–5	0–9	41	36–45	33–52	7.5	3.8
−36.3	6.0	400	FB	2	0	0–5	0–11	37	32–44	37–50	5.2	1.0
−47.0	302.0	450	FB	2	0	0–5	0–7	37	36–43	30–47	8.5	1.8
17.0	234.5	500	FB	3a	21	17–24	2–31	69	65–72	58–89	3.8	2.6
−45.7	278.2	300	RS	3a	0	0–12	0–16	65	53–73	47–77	3.2	5.8
−8.0	243.0	227	FB	3a	6	0–14	0–16	56	55–62	48–64	3.1	5.2
12.0	228.5	250	FB	3a	31	26–36	17–38	52	46–61	44–85	4.0	2.6
−7.5	221.5	600 × 300	FB	3a	45	42–47	40–56	42	38–45	34–50	2.8	1.9
57.5	255.0	330 × 150	RS	3a	0	0–7	0–11	40	34–46	30–52	3.6	3.6
−32.0	359.8	330	FB	3a	0	0–5	0–7	40	35–47	34–48	6.6	3.8
−27.0	31.0	300	FB	3a	6	0–16	0–18	33	24–46	22–52	3.5	11.8
−10.2	176.5	450 × 350	FB	3a	0	0–18	0–23	37	17–63	23–73	7.3	12.2
−33.4	303.6	290	FB	3a	34	21–40	12–43	32	24–62	22–75	1.9	3.4
14.2	15.4	300	RS	3a	6	0–14	0–16	31	25–42	22–45	1.1	2.9
9.0	262.0	450 × 350	PL	3a	0	0–5	0–7	50	47–57	45–60	7.2	2.2
−31.9	276.6	300 × 225	FB	3a	13	4–19	0–21	4	0–10	0–12	7.8	11.8
79.3	299.4	437 × 282	RS	3a	18	15–24	12–26	4	0–23	0–30	2.9	4.8
19.9	231.5	320	FB	3b	0	0–8	0–11	62	55–68	51–73	2.0	2.2
35.0	293.8	300 × 225	FB	3b	0	0–7	0–12	55	50–63	43–69	4.1	3.0
66.0	252.0	350 × 250	FB	3b	0	0–8	0–11	50	42–55	38–58	4.8	4.2
18.7	38.0	364	RS	3b	0	0–8	0–10	50	44–55	40–58	2.2	2.5
−68.0	357.0	780	FB	3b	0	0–5	0–8	34	30–36	26–40	6.1	4.7
52.8	259.3	515 × 480	RS	3b	3	0–11	0–14	30	25–39	21–44	5.2	6.7
−19.5	44.5	320	PL	3b	0	0–7	0–10	25	20–27	17–32	6.2	5.5
69.5	101.2	350 × 284	FB	3b	6	0–13	0–14	24	20–30	17–31	1.3	3.2
−8.0	8.6	360	FB	3b	16	0–19	0–20	11	7–26	5–30	8.5	10.2
27.0	35.0	320	FB	3b	16	8–18	0–20	10	5–21	4–26	3.5	4.6
77.1	277.3	430 × 340	RS	3b	9	4–15	0–17	13	7–18	5–23	4.0	3.7
10.0	246.0	200	FB	4	47	42–54	34–72	46	39–53	34–65	3.2	2.4
60.4	96.0	690 × 430	FB	4	6	0–16	0–19	25	17–42	13–46	4.9	8.3
31.7	241.3	385 × 295	FB	4	0	0–10	0–13	63	56–70	52–75	2.4	2.6
31.5	255.0	300	FB	4	0	0–10	0–14	62	51–69	46–74	3.3	3.9
31.5	258.3	315	FB	4	2	0–14	0–16	56	46–67	42–70	2.5	4.2
5.0	273.7	375 × 200	FB	4	0	0–9	0–15	54	44–63	37–70	4.7	3.8
11.0	248.5	300	FB	4	47	40–56	34–89	47	39–57	22–71	2.7	2.1
45.5	12.0	225	FB	4	3	0–15	0–18	41	32–58	26–65	3.4	5.4
19.5	153.5	220	FB	4	0	0–10	0–14	37	25–47	23–53	4.8	6.4
10.5	251.5	300	FB	4	48	44–52	42–60	30	29–42	22–50	1.0	1.4
18.5	125.0	250	PL	4	15	0–19	0–21	10	5–20	3–27	1.9	2.2
3.0	57.5	250 × 150	TE	4	10	0–16	0–18	10	3–21	0–25	4.4	7.8
40.8	271.9	271 × 263	RS	7	16	4–20	0–22	4	0–17	0–21	2.6	5.6
51.0	321.0	300 × 267	PL	7	19	5–20	0–24	2	0–17	0–27	6.8	6.4
−34.5	284.0	325 × 225	RS	7	0	0–6	0–9	47	40–50	36–55	9.9	8.2
21.0	84.5	320	PL	7	0	0–7	0–9	28	23–32	20–34	10.4	10.5
5.0	225.0	450 × 300	FB	8	45	40–55	30–60	21	13–46	7–55	2.3	2.1
3.5	233.7	225	FB	8	42	36–55	30–60	39	30–52	25–62	2.7	2.8
−4.0	210.5	260 × 200	FB	8	30	27–34	20–36	55	47–76	51–64	2.8	2.0
−3.5	215.0	300	FB	8	23	0–37	0–43	7	0–55	0–67	3.9	11.5
0.5	75.0	450	TE	8	10	0–16	0–19	10	3–20	0–24	2.9	4.1
48.7	247.0	380	PL	8	1	0–7	0–12	29	25–37	18–44	10.8	8.5

[a]Allowable ranges for T_e and Z_c are shown for RMS values of 1.5 times the observed RMS error. For comparison with *Barnett et al.* [2000], ranges are also shown for 2.0 times the RMS error. Parameters that lie within a range of 1.5 times the RMS for each spectrum are shown in the error plots in Figure 3b. See Table 1 caption for details of table contents.

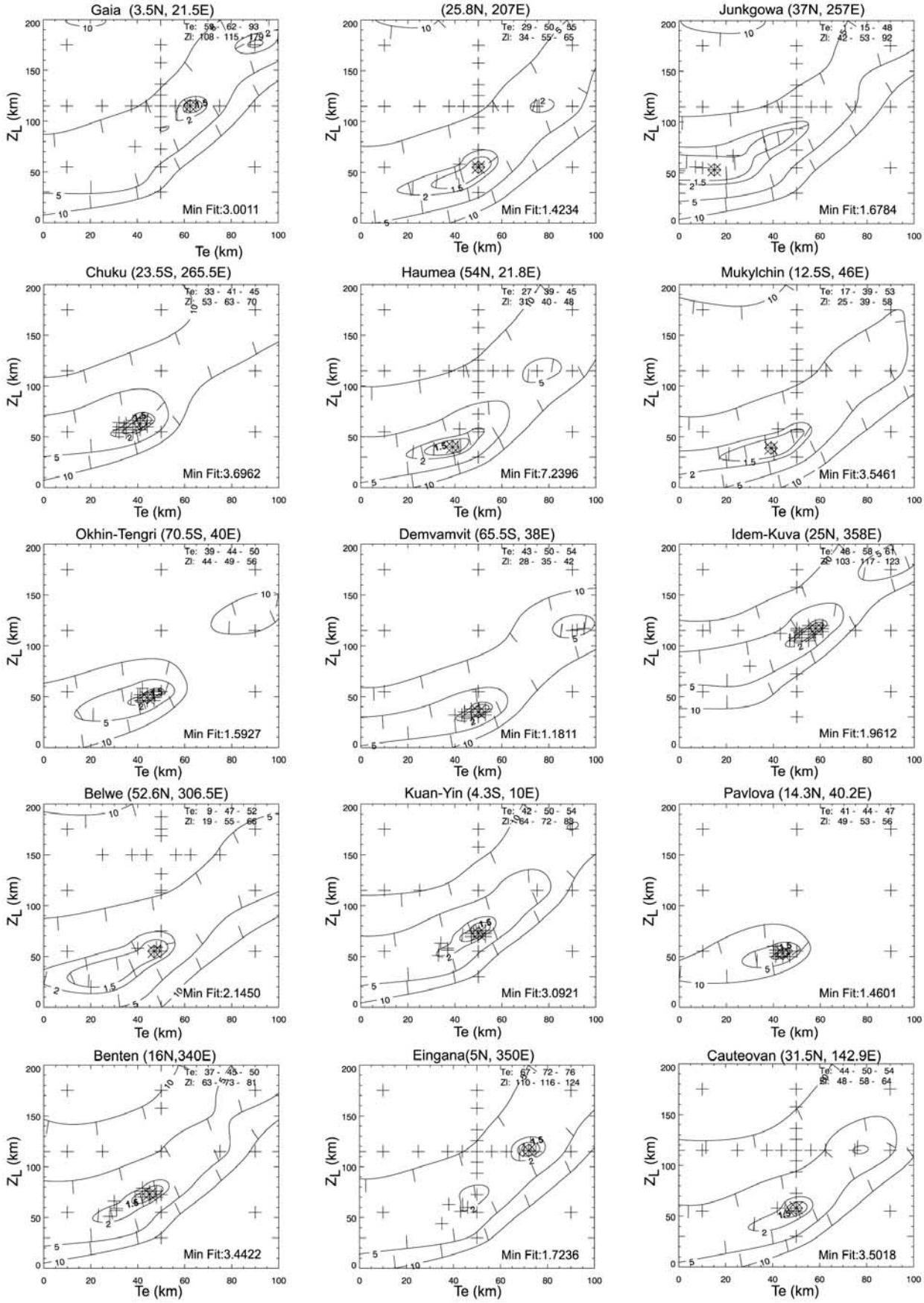
Gaia (3.5N, 21.5E)
Te: 58 - 62 - 93
ZI: 108 - 115 - 179
Min Fit:3.0011
(25.8N, 207E)
Te: 29 - 50 - 85
ZI: 34 - 55 - 65
Min Fit:1.4234
Junkgowa (37N, 257E)
Te: 33 - 15 - 48
ZI: 42 - 53 - 92
Min Fit:1.6784
Chuku (23.5S, 265.5E)
Te: 33 - 41 - 45
ZI: 53 - 63 - 70
Min Fit:3.6962
Haumea (54N, 21.8E)
Te: 27 - 39 - 45
ZI: 31 - 40 - 48
Min Fit:7.2396
Mukylchin (12.5S, 46E)
Te: 17 - 39 - 53
ZI: 25 - 39 - 58
Min Fit:3.5461
Okhin-Tengri (70.5S, 40E)
Te: 39 - 44 - 50
ZI: 44 - 49 - 56
Min Fit:1.5927
Demvamvit (65.5S, 38E)
Te: 43 - 50 - 54
ZI: 28 - 35 - 42
Min Fit:1.1811
Idem-Kuva (25N, 358E)
Te: 48 - 58 - 61
ZI: 103 - 117 - 123
Min Fit:1.9612
Belwe (52.6N, 306.5E)
Te: 9 - 47 - 52
ZI: 19 - 55 - 66
Min Fit:2.1450
Kuan-Yin (4.3S, 10E)
Te: 42 - 50 - 54
ZI: 64 - 72 - 88
Min Fit:3.0921
Pavlova (14.3N, 40.2E)
Te: 41 - 44 - 47
ZI: 49 - 53 - 56
Min Fit:1.4601
Benten (16N,340E)
Te: 37 - 43 - 50
ZI: 63 - 73 - 81
Min Fit:3.4422
Eingana(5N, 350E)
Te: 67 - 72 - 76
ZI: 110 - 116 - 124
Min Fit:1.7236
Cauteovan (31.5N, 142.9E)
Te: 44 - 50 - 54
ZI: 48 - 58 - 64
Min Fit:3.5018
Te (km)
Z_L (km)

Figure 3a.

from 30 to 117 km (Figures 5b and 5d, triangles). Some variation in Z_L may be due to the range of dynamic processes in coronae formation but the range is similar to those obtained in previous studies of other geological structures [*Janes and Squyres*, 1995; *Anderson and Smrekar*, 2001]. With the exception of one corona (26N, 97.7E), coronae with Z_L values greater than 70 km are located on Eistla Regio or on the surrounding planitia. Large values of Z_L in this region (>100 km) suggest that topography may be supported by thermal anomalies in the mantle and tends to rule out compensation due to crustal thickness variations. Most (~71%) of the coronae, however have Z_L estimates less than 70 km, indicating that compensation probably occurs within or at the base of the crustal layer. In these cases, compensation could be attributed to crustal density variations or to thickness variations, as discussed for Type 2 coronae [*Smrekar and Stofan*, 2003].

4.4. Topographic Morphology

[47] Coronae have previously been classified into 9 topographic groups [*Stofan et al.*, 1992; *Smrekar and Stofan*, 1997]. Table 3 and Figure 6 describe the different morphologies and summarize the lithospheric properties obtained here. Coronae in this survey cover the range of topographic morphologies with the exception of group 9. With only two examples, groups 5 and 6 are also underrepresented in the total corona population (6%) [*Stofan et al.*, 2001].

[48] Variations in corona morphology have been suggested to result from differences in mode of origin, variations in lithospheric structure and or regional or tectonic environment [*Stofan*, 1995] or from varying stages of development [*Smrekar and Stofan*, 1999]. We examine the range of elastic thickness values within each topographic group (Figure 5a). For top-loading group 1 (dome), 3b (rim surrounding an interior dome) and group 7 coronae (rim-only), the elastic thickness is less than 25 km, whereas for groups 2 (plateaus), 3a (rim surrounding interior high), 4 (rimmed depressions) and 8 (depressions) coronae interpreted using a top-loading model, T_e may vary from 0 to 40 km. Coronae with bottom-loading signatures show a generally larger range of T_e and more variability in elastic thickness with respect to topographic group, which may indicate actively evolving processes.

[49] Isostatic gravity signatures of perfect (Airy) isostatic compensation are found amongst all topographic morphologies. An isostatic signature implies that no dynamic processes are active. *Smrekar and Stofan* [2003] therefore suggest that any morphology can represent the final stage of coronae evolution. There is also no clear correlation between crustal thickness (for top-loading models) and topographic group (Figure 5b), implying that local thickness of the crust does not control coronae topography.

4.5. Geologic Setting and Geographic Location

[50] We also find no systematic relationship between values of T_e, Z_c, Z_L and geologic setting categorized as fracture belts, plains and rises (Figures 5c and 5d). A description of these geologic settings is given by *Stofan et al.* [1997]. *Glaze et al.* [2002] find that there is no apparent correlation between corona diameter and location in fracture belts or plains. Tesserae are generally agreed to be mainly isostatically supported [e.g., *Bindschadler et al.*, 1992; *McKenzie*, 1994] and hence have a lower T_e than average. Only two coronae located in tesserae regions are included in this study. Both of these coronae show small values of T_e and Z_c.

[51] Typically the apparent depth of compensation of coronae at rises is smaller than average values for Venus [*Smrekar and Phillips*, 1991; *McKenzie and Nimmo*, 1997; *Simons et al.*, 1997; *Barnett et al.*, 2000]. Rises have been suggested as hot spot locations given their domed topography and associated volcanism [*Smrekar et al.*, 1997]. Large, long wavelength apparent depths of compensation obtained at hot spot rises have previously been interpreted as evidence that a hot spot is still active [*Smrekar and Phillips*, 1991; *Simons et al.*, 1997]. We find that four of the seven bottom-loading coronae located on rises have Z_L values less than 80 km, suggesting that their behavior is distinct from that of the topographic rises as a whole.

[52] All 17 coronae modeled as top-loading with elastic thickness estimates greater than 20 km are located at the junction between Hecate and Parga chasmata, which may indicate that these two chasmata are sites of active deformation.

[53] *Johnson and Richards* [2003] infer a group of coronae to be comparatively young on the basis of positive gravity anomalies that they attribute to support by a combination of mantle dynamics and strong lithospheric flexure. These coronae are termed ''uncompensated''. Although they use a different method to determine whether a corona is compensated or uncompensated, they found that these uncompensated coronae are also concentrated predominantly in the Beta-Atla-Themis (BAT) [*Stofan et al.*, 1992] region which includes the junction of Hecate and Parga Chasma. We find however, that bottom-loaded (uncompensated) coronae are found in most regions with the exception of that spanned by longitudes 100°E–200°E, and previously identified as coronae deficient [*Stofan et al.*, 2001]. *Johnson and Richards* [2003] identify a class of older coronae on the grounds that their topography is ''compensated'' and their free-air gravity anomaly is near zero. These coronae are globally distributed. Similarly, we find that coronae with isostatically compensated signatures are found across all geologic settings and are distributed globally (Figure 7).

4.6. Coronae Diameter

[54] The diameters of coronae examined in this survey range from 200–1060 km. *Stofan et al.* [1992, 2001] measure the maximum diameter of coronae using the largest distance between the outermost fractures of the annuli.

Figure 3a. RMS model misfits (units of mgal/km) are shown for bottom-loading models in the $Z_L - T_e$ plane. X marks the location of the best fit value. RMS misfit in each plot is normalized by the RMS variation in the observed admittance spectra.

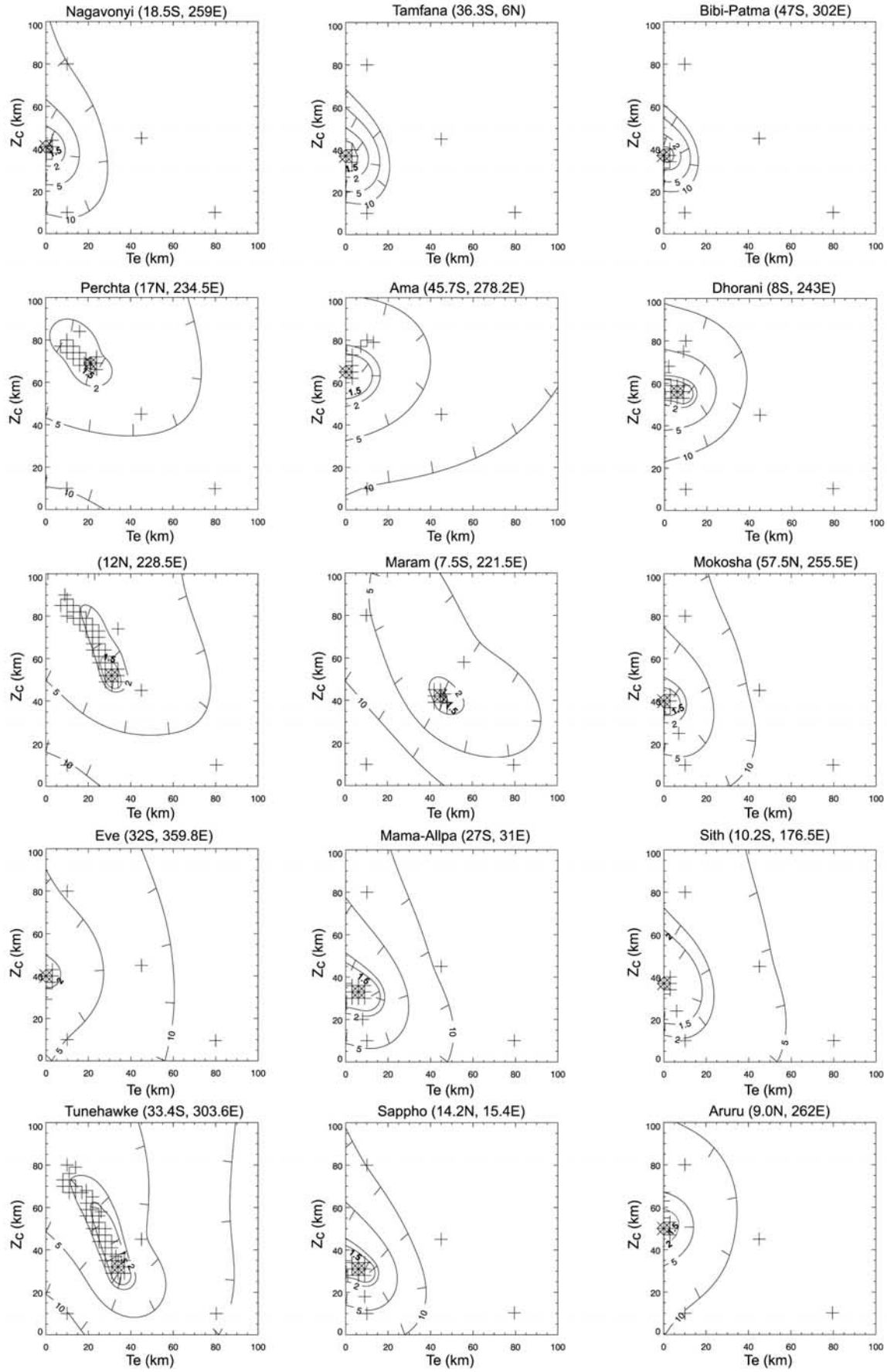
Nagavonyi (18.5S, 259E)
Tamfana (36.3S, 6N)
Bibi-Patma (47S, 302E)
Perchta (17N, 234.5E)
Ama (45.7S, 278.2E)
Dhorani (8S, 243E)
(12N, 228.5E)
Maram (7.5S, 221.5E)
Mokosha (57.5N, 255.5E)
Eve (32S, 359.8E)
Mama-Allpa (27S, 31E)
Sith (10.2S, 176.5E)
Tunehawke (33.4S, 303.6E)
Sappho (14.2N, 15.4E)
Aruru (9.0N, 262E)
Zc (km)
Te (km)

Figure 3b.

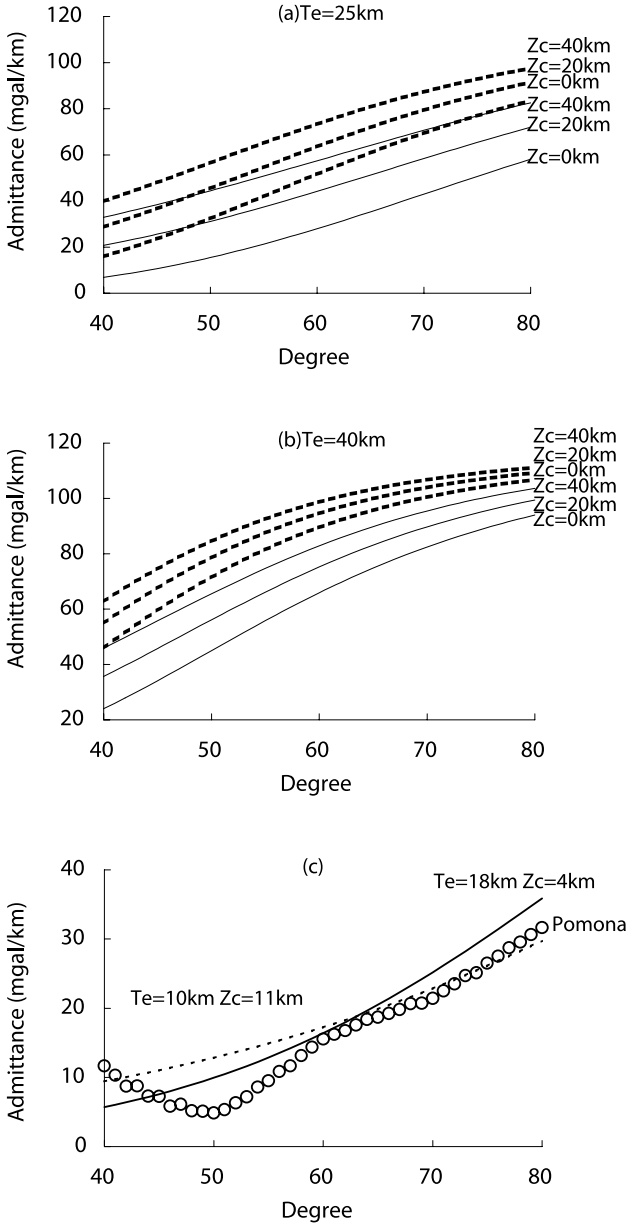

Figure 4. Model admittance spectra show the effect of crust-mantle density contrast for top-loading T_e values of (a) 25 km and (b) 40 km and a range of Z_c values. Crust-mantle density contrasts of 500 kg/m^3 and 200 kg/m^3 are represented as solid and dashed lines respectively. The observed admittance for (c) Pomona corona (79.3N 299.4) is represented by circles between degree 40 and 80. Best fit elastic and crustal thickness estimates for each density contrast are also shown.

McGovern and Solomon [1998] suggested that elastic thickness acts as a filter to corona formation, with larger coronae forming in regions of thicker elastic lithosphere. Regardless of compensation model, we find no significant correlation between diameter and T_e (Figure 8), suggesting that elastic thickness does not influence coronae size.

4.7. Models of Corona Formation

[55] Early models of corona formation included: Rising diapir (plume model), sinking diapir and gravitational relaxation of topography [*Stofan et al.*, 1991]. The morphology, volcanism and pattern of fractures found at coronae led *Stofan et al.* [1991] to conclude that they form over mantle diapirs. Further investigations focused on the rising diapir (plume) model [e.g., *Janes et al.*, 1992] including modification by topographic relaxation [*Janes and Squyres*, 1995] and loading of the lithosphere by volcanism [*Cyr and Melosh*, 1993]. *Koch and Manga* [1996] described a corona formation model involving a diapir spreading at a depth of neutral buoyancy. In this model, a diapir with uniform density and viscosity rises in a 2-layer medium where both layers have uniform viscosity. *Smrekar and Stofan* [1997] developed a formation model that includes delamination and a depleted mantle layer at depth to produce the observed range of coronae topography. In this axisymmetric finite element model, Newtonian viscosity is temperature-dependant and is parameterized such that the viscosity of the plume and lower lithosphere cover a plausible range with a uniform viscosity in the uppermost lithosphere [*Smrekar and Stofan*, 2003]. Of these models, only the spreading-drop model and the plume-delamination model predict the interior depressions which form almost half of the corona population [*Glaze et al.*, 2002].

4.8. Implications for Models of Corona Formation

[56] The lithospheric parameters calculated in this paper were compared with predictions made by different corona formation models. Plume models predict positive topography (e.g., domes, plateaus) with large apparent depths of compensation while the plume is active. If coronae form over mantle plumes, local thinning of the lithosphere may occur and smaller values of T_e are predicted. Our results suggest that few if any dome or plateau shaped coronae have the combination of thin elastic thickness, large compensation depths, and bottom-loading signatures consistent with their being supported by an active plume. If these coronae are underlain by active plumes, they do not cause a reduction in elastic thickness or an increase in compensation depth. It is possible that smaller plumes may not produce large apparent depths of compensation or cause thinning of the elastic layer. The majority of coronae with positive topography (groups 1, 2, 3a) examined here, are apparently approaching an isostatic state or they display relatively large values of elastic thickness.

[57] The plume/delamination model [*Smrekar and Stofan*, 1997] predicts a top-loading signature when delamination occurs. Most coronae with interior depressions (67% of group 4 and 100% of group 8), display admittance signatures consistent with top-loading. Given their depressed topography, these coronae are inconsistent with a plume model of formation which may suggest that delamination (or gravitational instability) is active. An alternative corona

Figure 3b. RMS model misfits (units of mgal/km) are shown for top-loading models in the $Z_c - T_e$ plane. X marks the location of the best fit value. RMS misfit in each plot is normalized by the RMS variation in the observed admittance spectra.

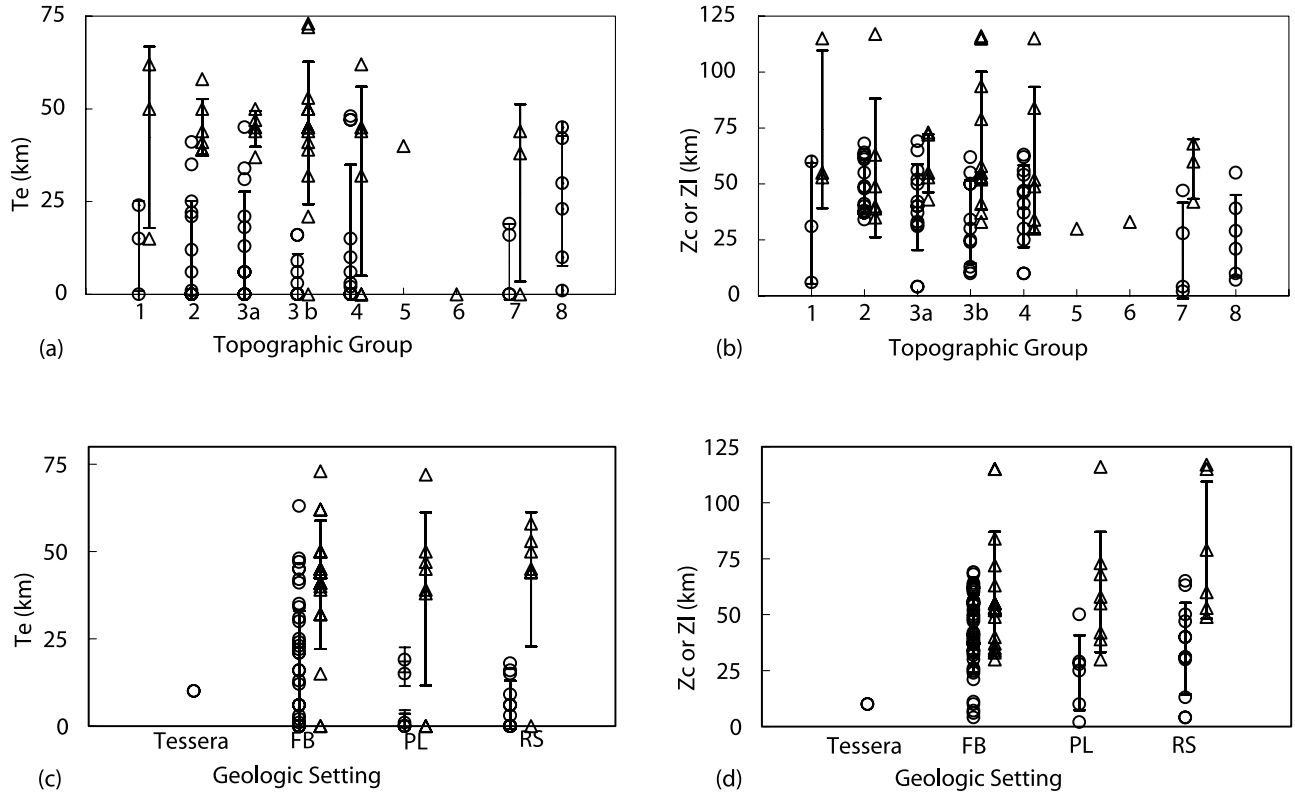

Figure 5. Elastic thickness (T_e) is shown versus topographic group (a) and geologic setting (c). Crustal thickness (Z_c) for top-loading models (circles) and lithospheric thickness (Z_L) for bottom-loading models (triangles) are also shown versus geologic setting (b) and topographic group (d). FB, PL and RS in (c) and (d) represent fracture belts, plains, and rises. The topographic morphology groups are shown in Table 3 and Figure 6 [*Smrekar and Stofan*, 1997]. For both bottom and top-loading models, error bars represent one standard deviation.

formation model includes the gravitational (Rayleigh-Taylor) instability of the dense mantle lithosphere [*Tackley and Stevenson*, 1991; *Tackley et al.*, 1992; *Hamilton and Stofan*, 1996; *Hoogenboom and Houseman*, 2002]. Rayleigh-Taylor instability is expected to produce a similar admittance signature to delamination. Future work should assess the predicted admittance signature and likelihood of Rayleigh-Taylor instability as a formation mechanism.

[58] The spreading-drop model [*Koch and Manga*, 1996] suggests that the ratio of crustal thickness to diapir diameter is important in controlling morphology. Following *Smrekar et al.* [2003] we test this hypothesis by plotting the ratio of crustal thickness to corona diameter versus coronae diameter (Figure 9) as a proxy for crustal thickness over plume diameter. For constant crustal thickness, this graph shows a hyperbolic relation as represented by the solid lines for Z_c values of 10, 25, 50 and 70 km. With the exception of plateau shaped coronae which are scattered about the Z_c = 50 km curve, none of the topographic groups display a clear relationship between crustal thickness/diameter and diameter. Most of the coronae are scattered between the 10 and 70 km curves. *Koch and Manga* [1996] predict that appreciable coronae surface deformation will not be produced for Z_c/diapir radius values larger than ~0.4. This is equivalent to a maximum Z_c/diameter value of 0.27 based on the suggestion by

Table 3. Mean, Standard Deviation, and Range of Elastic Thickness (T_e), Crustal Thickness (Z_c), and Lithospheric Thickness (Z_L) for All (98) Resolvable Type 1 Coronae Obtained Using Top- and Bottom-Loading Models[a]

	Top Loading		Bottom Loading	
Group	T_e (km), Mean ± St. Dev., Range	Z_c (km), Mean ± St. Dev., Range	T_e (km), Mean ± St. Dev., Range	Z_L (km), Mean ± St. Dev., Range
1	13 ± 12 (3) 0–24	32 ± 27 (3) 6–60	42 ± 24 (3) 15–62	74 ± 35 (3) 53–115
2	11 ± 14 (15) 0–41	49 ± 12 (15) 34–68	45 ± 8 (6) 39–58	57 ± 31 (6) 35–117
3a	13 ± 15 (14) 0–45	40 ± 19 (14) 4–69	45 ± 5 (5) 37–50	59 ± 13 (5) 43–73
3b	5 ± 6 (11) 0–16	33 ± 19 (11) 10–62	43 ± 19 (10) 0–73	69 ± 31 (10) 33–116
4	15 ± 20 (12) 0–48	40 ± 18 (12) 10–63	31 ± 25 (6) 0–62	61 ± 33 (6) 30–115
5	(0)	(0)	40 (1)	30 (1)
6	(0)	(0)	0 (1)	33 (1)
7	9 ± 10 (4) 0–19	20 ± 21 (4) 2–47	27 ± 24 (3) 0–44	57 ± 13 (3) 42–68
8	25 ± 17 (6) 1–45	27 ± 18 (6) 7–55	(0)	(0)
9	(0)	(0)	(0)	(0)

[a]Numbers in parentheses refer to the number of coronae in each topographic group for which we have obtained estimates of lithospheric properties.

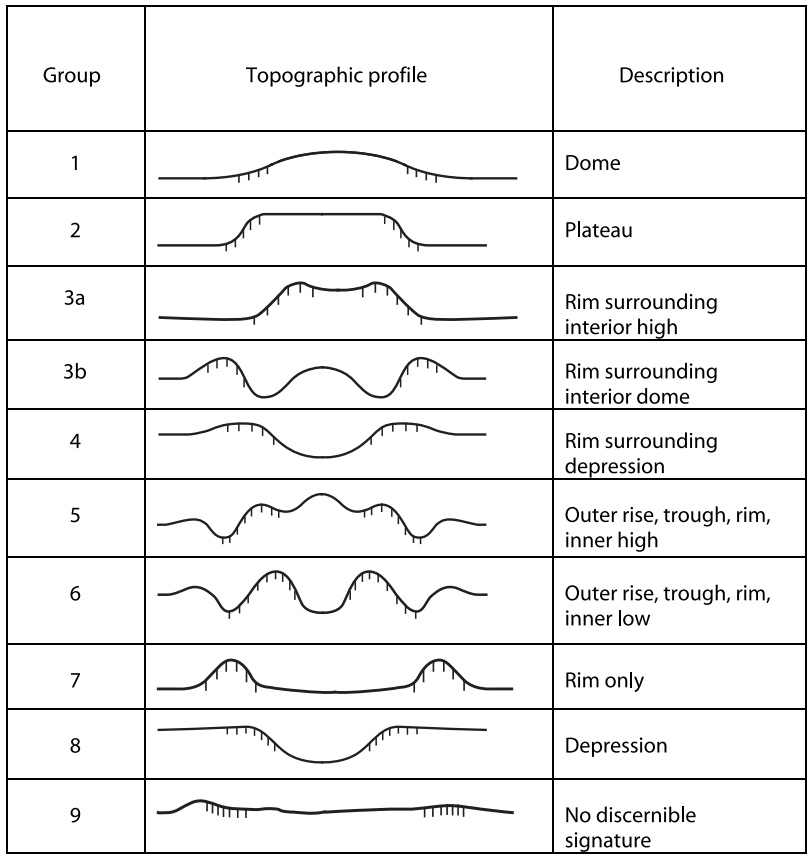

Figure 6. Topographic group classification for coronae on Venus. Vertical tick marks on topographic profiles indicate the typical location of annuli for each group (adapted from *Smrekar and Stofan* [1997]).

Smrekar and Stofan [2003] that the corona diameter ratio is likely to be a factor of up to 2 greater than the initial diapir diameter. In agreement with the spreading-drop model, all the Type 1 coronae fall below this value. However, the spreading-drop model predicts that for a given crustal thickness, there should be a progression in coronae diameter from domes, to plateaus, to rim-only forms, to rimmed depressions. We observe no such progression (Figure 9). We find that rim-only (group 7) coronae are predominantly isostatic, consistent with both the spreading-drop model (which forms rim-only coronae through extreme spreading of the plume head) and the plume-delamination model (which forms rim-only coronae via isostatic rebound of a low density layer following delamination).

[59] Most of the coronae could be interpreted as implying compensation in the crustal layer. The crustal thickness values estimated here for coronae fit with a top-loading model suggest significant regional variability in crustal thickness and possibly density. The mechanism by which crustal thickness changes (whether thickening/thinning or phase change such as basalt-eclogite) remains unclear however, as does the manner in which crustal thickness variation might influence corona formation. Some of the more complex topographic forms like rim surrounding interior domes (group 3b) and rim surrounding depressions (group 4) display large T_e and mostly intermediate Z_c and Z_L values, which implies compensation within the crustal layer. Large ranges of Z_L could also imply laterally variable vertical density variation.

4.9. Comparison Between Type 1 and Type 2 Coronae

[60] *Stofan et al.* [2001] proposed a series of hypotheses to explain the relative lack of fracture annuli at Type 2 coronae. These include the presence of a purely ductile lithosphere due to high heat flux, strong lithosphere and thus low strain rate and slow viscous bending at the surface. *Stofan et al.* [2001] suggest that unrealistically high values of heat flux would be needed to move the brittle-ductile transition to the surface. Table 4 provides a comparison of lithospheric parameters inferred for Type 1 and 2 coronae. Type 1 and 2 coronae [*Smrekar et al.*, 2003] form on lithosphere with a wide range of T_e, therefore low strain rate deformation can not be due to a simple difference in elastic thickness. *Johnson and Sandwell* [1994] also infer low strain rates due to large elastic thickness that they obtained for some Type 1 coronae. On the basis of our results, if low strain rate deformation is responsible for the lack of full annulus development at Type 2 coronae, it must be due to variation in the formation process rather than differences in the crustal or elastic thickness.

[61] Only topographic groups 4 and 7 contain enough coronae in each Type to compare elastic thickness values with topographic morphology. Type 1 rimmed depressions (Group 4) display elastic thickness values between 0 and 62 km (Figure 5a) whereas Type 2 (Group 4) coronae

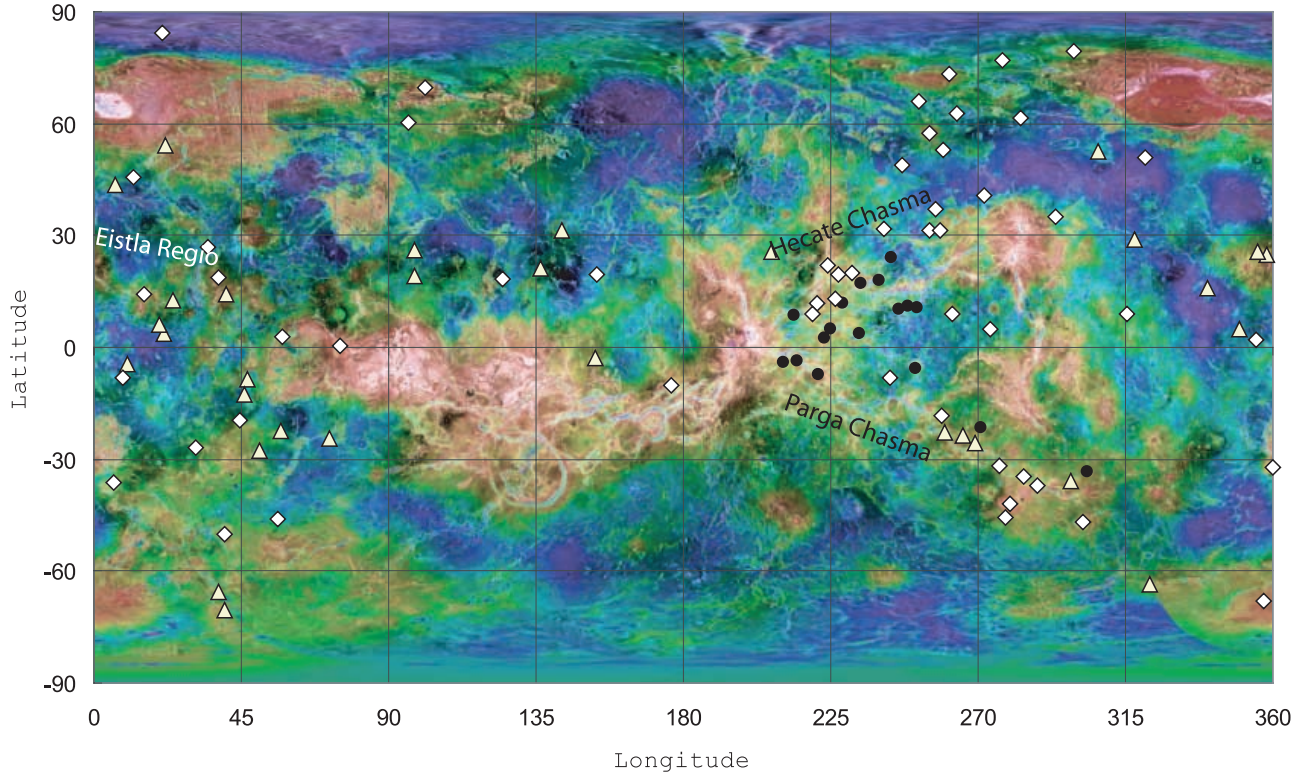

Figure 7. Geographical distribution of coronae best fit by the different loading models. Triangles represent coronae best fit with a bottom-loading model, circles represent coronae best fit with a top-loading model and diamonds represent coronae interpreted to be isostatically compensated.

display values between 0 and ~80 km (Table 4). Similarly, Type 1 rim-only coronae (Group 7) display elastic thickness values between 0 and 44 km whereas Type 2 rim-only coronae display values between 0 and ~60 km. The differences between these ranges of elastic thickness from Type 1 and 2 are relatively small when we consider the allowable range of error estimates.

[62] Approximately 54% of Type 1 coronae are interpreted to be isostatic. Similarly ~47% of Type 2 coronae are also interpreted to be isostatic. Again, the difference in this statistic is probably not significant. Given the similar ranges of Z_c and Z_L values, neither crustal thickness nor apparent depth of compensation appears to constrain whether a corona has a complete (Type 1) or partial (Type 2) annulus of deformation features.

5. Conclusions

[63] This survey provides a quantitative assessment of lithospheric properties associated with Type 1 coronae and

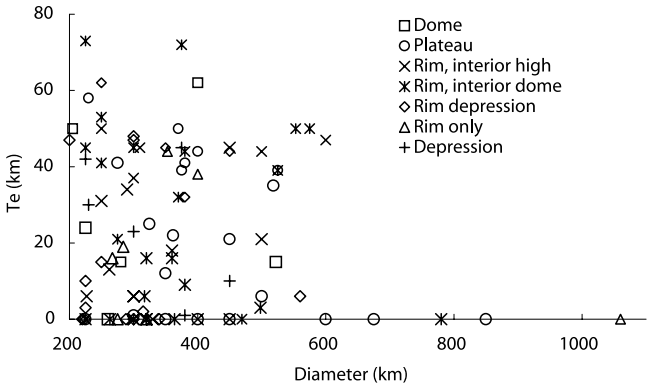

Figure 8. Elastic thickness estimates for each topographic morphology (refer key) are shown versus coronae diameter. Smaller symbols denote coronae best fit with the bottom-loading model. Elastic thickness does not appear to constrain the diameter of Type 1 coronae.

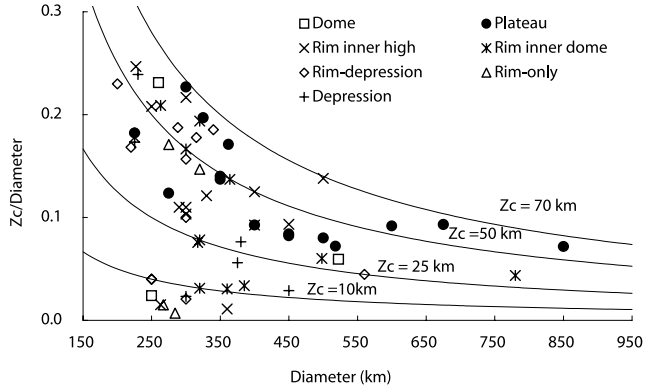

Figure 9. The ratio of crustal thickness (Z_c) to corona diameter is plotted against diameter. The symbol shape indicates the topographic morphology of the corona as indicated. Solid lines represent the relation for a constant value of crustal thickness as labeled.

Table 4. Comparison of Lithospheric Parameter Estimates Between Type 1 and Type 2 Coronae[a]

	Type 1		Type 2	
	Mean ± Std. Dev.	Best Fit Range	Mean ± Std. Dev.	Best Fit Range
Z_c, km	38 ± 19	2–69	44 ± 29	5–130
T_e, km	22 ± 21	0–73	32 ± 27	0–80
Z_L, km	63 ± 28	30–117	86 ± 28	49–140

[a]*Smrekar et al.* [2003]. Average values of T_e include measurement from both types of compensation model.

demonstrates that these coronae display the same range of elastic thicknesses observed for other Venusian topographic features. Crustal thickness and apparent depth of compensation estimates are also similar to those found for other Venusian geological structures, suggesting that the lithosphere on which coronae form is not unique. 54% of Type 1 and 2 coronae are consistent with local isostasy, which we interpret to indicate that these coronae are no longer active. Very few dome or plateau shaped coronae have the combination of thin elastic thickness, large compensation depths, and bottom-loading signatures expected if these features are supported by active plumes. Coronae located on and around Eistla Regio are distinguished by their large depths of compensation. Approximately 71% of the coronae have Z_L estimates less than 70 km, indicating that compensation probably occurs within the crustal layer. In these cases, compensation could be attributed to crustal density variations or thickness variations. Differences in deformation pattern between Type 1 and 2 coronae do not appear to result from variations in elastic thickness but are inferred to result from Type 2 coronae forming with a low strain rate that inhibits brittle deformation at the surface. We find no clear relationship between elastic thickness or crustal thickness and coronae diameter, as predicted by the spreading-drop model of coronae formation. These results highlight the role of crustal thickness and possibly density variations in the compensation, evolution and morphology of coronae.

[64] **Acknowledgments.** We thank E. R. Stofan for supplying the updated coronae database and M. Simons for the use of his spatio-spectral localization method. C. Ebinger and an anonymous reviewer are gratefully acknowledged for their helpful and thorough reviews. P. Grindrod is thanked for assistance with Figure 7. The research described in this paper was carried out at the Jet Propulsion Laboratory, California Institute of Technology, under a contract with the National Aeronautics and Space Administration. S. Smrekar was supported by a grant from the National Aeronautics and Space Administration's planetary geology and geophysics program.

References

Anderson, F. S., and W. B. Banerdt (2000), Preliminary admittance estimates for the Valles Marineris, Mars, *Lunar Planet. Sci.* [CD-ROM], *XXXI*, abstract 2090.

Anderson, F. S., and S. E. Smrekar (2001), Global admittance estimates of elastic and crustal thickness of Venus: Preliminary results from top and bottom-loading models, *Lunar Planet. Sci.* [CD-ROM], *XXXII*, abstract 2182.

Banks, R. J., and C. J. Swain (1978), The isostatic compensation of East Africa, *Proc. R. Soc. London, Ser. A*, *364*, 331–352.

Banks, R. J., S. C. Francis, and R. G. Hipkin (2001), Effects of loads in the upper crust on estimates of elastic thickness of the lithosphere, *Geophys. J. Int.*, *145*, 291–299.

Barnett, D. N., F. Nimmo, and D. McKenzie (2000), Flexure of Venusian lithosphere measured from residual topography and gravity, *Icarus*, *16*, 404–419.

Bindschadler, D. L., G. Schubert, and W. M. Kaula (1992), Coldspots and hotspots: Global tectonics and mantle dynamics of Venus, *J. Geophys. Res.*, *97*, 13,495–13,582.

Brown, C. D., and R. E. Grimm (1996), Lithospheric rheology and flexure at Artemis Chasma, Venus, *J. Geophys. Res.*, *101*, 12,697–12,708.

Cyr, K. E., and H. J. Melosh (1993), Tectonic patterns and regional stresses near Venusian coronae, *Icarus*, *102*, 175–184.

Dorman, L. M., and B. T. R. Lewis (1970), Experimental isostasy: 1. Theory of the determination of the Earth's isostatic response to a concentrated load, *J. Geophys. Res.*, *75*, 3357–3365.

Forsyth, D. W. (1985), Sub-surface loading and estimates of the flexural rigidity of the continental lithosphere, *J. Geophys. Res.*, *90*, 12,623–12,632.

Glaze, L. S., E. R. Stofan, S. E. Smrekar, and S. M. Baloga (2002), Insights into corona formation through statistical analyses, *J. Geophys. Res.*, *107*(E12), 5135, doi:10.1029/2002JE001904.

Grimm, R. E., and P. C. Hess (1997), The crust of Venus, in *Venus II*, edited by S. W. Bougher, D. M. Hunten, and R. J. Phillips, pp. 1205–1244, Univ. of Ariz. Press, Tucson.

Hamilton, V., and E. R. Stofan (1996), The geomorphology and evolution of Hecate Chasma, Venus, *Icarus*, *121*, 171–194.

Hoogenboom, T., and G. Houseman (2002), Rayleigh-Taylor Instabilities as a mechanism for coronae formation on Venus, *Eos Trans. AGU*, *83*(47), Fall Meet. Suppl., Abstract P71B-0466.

Janes, D. M., and S. W. Squyres (1995), Viscoelastic relaxation of topographic highs on Venus to produce coronae, *J. Geophys. Res.*, *100*(E8), 21,173–21,188.

Janes, D. M., S. W. Squyres, D. L. Bindschadler, G. Baer, G. Schubert, V. L. Sharpton, and E. R. Stofan (1992), Geophysical models for the formation and evolution of coronae on Venus, *J. Geophys. Res*, *97*, 16,055–16,067.

Johnson, C. L., and M. A. Richards (2003), A conceptual model for the relationship between coronae and large-scale mantle dynamics on Venus, *J. Geophys. Res.*, *108*(E6), 5058, doi:10.1029/2002JE001962.

Johnson, C. L., and D. T. Sandwell (1994), Lithospheric flexure on Venus, *Geophysics J. Int.*, *119*, 627–647.

Kiefer, W. S. (2000), Gravity anomalies at Venus shield volcanoes: Implications for lithospheric thickness, *Lunar Planet. Sci, XXXI*, abstract 1924.

Koch, D. M., and M. Manga (1996), Neutrally buoyant diapirs: A model for Venus coronae, *Geophys. Res. Lett.*, *23*, 220–228.

Konopliv, A. S., W. S. Banerdt, and W. L. Sjogren (1999), Venus gravity: 180th degree and order model, *Icarus*, *139*, 3–18.

Lowry, A. R., and R. B. Smith (1994), Flexural rigidity of the Basin and Range-Colorado Plateau-Rocky Mountain transition from coherence analysis of gravity and topography, *J. Geophys. Res.*, *99*(B10), 20,123–20,140.

Lowry, A. R., and R. B. Smith (1995), Strength and rheology of the western U.S. Cordillera, *J. Geophys. Res.*, *100*, 17,947–17,963.

McGovern, P. J., and S. C. Solomon (1998), Growth of large volcanoes on Venus: Mechanical models and implications for structural evolution, *J. Geophys. Res.*, *103*, 11,071–11,101.

McKenzie, D. (1994), The relationship between topography and gravity on Earth and Venus, *Icarus*, *112*, 55–88.

McKenzie, D. (2003), Estimating T_e in the presence of internal loads, *J. Geophys. Res.*, *108*(B9), 2438, doi:10.1029/2002JB001766.

McKenzie, D., and D. Fairhead (1997), Estimates of the effective elastic thickness of the continental lithosphere from Bouguer and free air gravity anomalies, *J. Geophys. Res.*, *102*(B12), 27,523–27,552.

McKenzie, D., and F. Nimmo (1997), Elastic thickness estimates for Venus from line of sight accelerations, *Icarus*, *130*, 198–216.

McNutt, M. K. (1983), Influence of plate subduction on isostatic compensation in northern California, *Tectonics*, *2*, 399–415.

Moresi, L., and B. Parsons (1995), Interpreting gravity, geoid and topography for convection with temperature dependent viscosity: Application to surface features on Venus, *J. Geophys. Res.*, *100*, 21,155–21,171.

Nimmo, F., and D. McKenzie (1996), Modelling plume-related uplift, gravity and melting on Venus, *Earth Planet. Sci. Lett.*, *145*, 109–123.

Petit, C., and C. Ebinger (2000), Flexure and mechanical behavior of carbonic lithosphere: Gravity models of the East African and Baikal Rifts, *J. Geophys. Res.*, *15*, 19,151–19,162.

Rappaport, N. J., A. S. Konopliv, A. B. Kucinskas, and P. G. Ford (1990), An improved 360 degree and order model of Venus topography, *Icarus*, *139*, 19–30.

Sandwell, D. T., and G. Schubert (1992), Flexural ridges, trenches, and outer rises around Venus coronae, *J. Geophys. Res.*, *97*, 16,069–16,083.

Simons, F. J., M. T. Zuber, and J. C. Korenaga (2000), Isostatic response of the Australian lithosphere: Estimation of effective elastic thickness and anisotropy using multitaper spectral analysis, *J. Geophys. Res.*, *105*, 19,163–19,184.

Simons, M., B. H. Hager, and S. C. Solomon (1994), Global variations in geoid/topography admittances on Venus, *Science*, *256*, 798–803.

Simons, M., S. C. Solomon, and B. H. Hager (1997), Localization of the gravity and topography constraints on the tectonics and mantle dynamics of Venus, *Geophysics J. Int.*, *131*, 24–44.

Smrekar, S. E., and R. J. Phillips (1991), Venusian highlands: Geoid to topography ratios and their implications, *Earth Planet. Sci. Lett.*, *107*, 582–597.

Smrekar, S. E., and E. R. Stofan (1997), Corona formation and heat loss on Venus by coupled upwelling and delamination, *Science*, *277*, 1289–1294.

Smrekar, S. E., and E. R. Stofan (1999), Origin of corona-dominated topographic rises on Venus, *Icarus*, *139*, 100–115.

Smrekar, S. E., and E. R. Stofan (2003), Effects of lithospheric properties on the formation of Type 2 coronae on Venus, *J. Geophys. Res.*, *108*(E8), 5091, doi:10.1029/2002JE001930.

Smrekar, S. E., E. R. Stofan, and W. S. Kiefer (1997), Large volcanic rises on Venus, in *Venus II*, edited by S. W. Bougher, D. M. Hunten, and R. J. Phillips, pp. 845–878, Univ. of Ariz. Press, Tucson.

Smrekar, S. E., R. Comstock, and F. S. Anderson (2003), A gravity survey of Type 2 coronae on Venus, *J. Geophys. Res.*, *108*(E8), 5090, doi:10.1029/2002JE001935.

Stofan, E. R. (1995), Coronae on Venus: Topographic variations and correlations between morphology and regional setting (abstract), *Lunar Planet. Sci.*, *XXVI*, 1361–1362.

Stofan, E. R., D. L. Bindschadler, J. W. Head, and E. M. Parmentier (1991), Corona structures on Venus: Models of origin, *J. Geophys. Res.*, *96*(E4), 20,933–20,946.

Stofan, E. R., V. L. Sharpton, G. Schubert, G. D. Baer, D. L. Bindschadler, D. M. Janes, and S. W. Squyres (1992), Global distribution and characteristics of coronae and related features on Venus: Implications for origin and relation to mantle processes, *J. Geophys. Res.*, *97*, 13,347–13,378.

Stofan, E. R., V. E. Hamilton, D. M. Janes, and S. E. Smrekar (1997), Coronae on Venus, in *Venus II*, edited by S. W. Bougher, D. M. Hunten, and R. J. Phillips, pp. 931–965, Univ. of Ariz. Press, Tucson.

Stofan, E. R., S. E. Smrekar, S. W. Tapper, J. E. Guest, and P. Grinrod (2001), Preliminary analysis of an expanded corona database for Venus, *Geophys. Res. Lett.*, *28*, 4267–4270.

Tackley, P. J., and D. J. Stevenson (1991), The production of small Venusian coronae by Rayleigh Taylor instabilities in the uppermost mantle, *Eos Trans. AGU*, *72*, 287.

Tackley, P. J., D. J. Stevenson, and D. R. Scott (1992), Volcanism by melt driven Rayleigh Taylor instabilities and possible consequences of melting for admittance ratios on Venus (abstract), in *Papers Presented to the International Colloquium on Venus*, *LPI Contrib. 789*, pp. 123–124, Lunar and Planet. Inst., Houston, Tex.

Wang, Y., and J. C. Mareschal (1999), Elastic thickness of the lithosphere in the central Canadian shield, *Geophys. Res. Lett.*, *26*(19), 3033–3035.

Watts, A. B., J. H. Bodine, and M. S. Steckler (1980), Observations of flexure and the state of stress in the oceanic lithosphere, *J. Geophys. Res.*, *85*(B11), 6369–6376.

Zuber, M. T., and E. M. Parmentier (1990), On the relationship between isostatic elevation and the wavelengths of tectonic surface features on Venus, *Icarus*, *85*, 290–308.

Zuber, M. T., T. D. Bechtel, and W. D. Forsyth (1989), Effective elastic thickness of the lithosphere and mechanisms of isostatic compensation in Australia, *J. Geophys. Res.*, *94*, 13,930.

F. S. Anderson, Hawaii Institute of Geophysics and Planetology, University of Hawaii at Manoa, 1680 East-West Road, Post 602B, Honolulu, HI 96822, USA.

T. Hoogenboom and G. Houseman, School of Earth Sciences, University of Leeds, Woodhouse Lane, Leeds LS2 9JT, UK. (trudi@earth.leeds.ac.uk)

S. E. Smrekar, Jet Propulsion Laboratory, 4800 Oak Grove Drive, Mail Stop 183-501, Pasadena, CA 91109, USA.